Time-Dependent Long-Range-Corrected Double-Hybrid Density Functionals with Spin-Component and Spin-Opposite Scaling: A Comprehensive Analysis of Singlet-Singlet and Singlet-Triplet Excitation Energies

Marcos Casanova-Páez* and Lars Goerigk*

School of Chemistry, The University of Melbourne, Parkville, Victoria 3010, Australia

E-mail: mcasanova@student.unimelb.edu.au; lars.goerigk@unimelb.edu.au
Phone: +61 3 834 46784

Abstract

Following the work on spin-component and spin-opposite scaled (SCS/SOS) global double hybrids for singlet-singlet excitations by Schwabe and Goerigk [*J. Chem. Theory Comput.* **2017**, *13*, 4307-4323] and our own works on new long-range corrected (LC) double hybrids for singlet-singlet and singlet-triplet excitations [*J. Chem. Theory Comput.* **2019**, *15*, 4735-4744; *J. Chem. Phys.* **2020**, *153*, 064106], we present new LC double hybrids with SCS/SOS that demonstrate further improvement over previously published results and methods. We introduce new unscaled and scaled versions of different global and LC double hybrids based on Becke88 or PBE exchange combined with LYP, PBE or P86 correlation. For singlet-singlet excitations, we cross-validate them on six benchmark sets that cover small to medium-sized chromophores with different excitation types (local valence, Rydberg, and charge transfer). For singlet-triplet excitations, we perform the cross-validation on three different benchmark sets following the same analysis as in our previous work in 2020. In total, 203 unique excitations are analyzed. Our results confirm and extend those of Schwabe and Goerigk regarding the superior performance of SCS and SOS variants compared to their unscaled parents by decreasing mean absolute deviations, root-mean-square deviations or error spans by more than half and bringing absolute mean deviations closer to zero. Our SCS/SOS variants show to be highly efficient and robust for the computation of vertical excitation energies, which even outperform specialized double hybrids that also contain an LC in their perturbative part. In particular, our new SCS/SOS-ωPBEPP86 and SCS/SOS-ωB88PP86 functionals are four of the most accurate and robust methods tested in this work and we fully recommend them for future applications. However, if the relevant SCS and SOS algorithms are not available to the user, we suggest ωPBEPP86 as the best unscaled method in this work.

1 Introduction

Density functional theory (DFT) is nowadays the most widely used methodology for the computation of ground state properties given its good compromise between accuracy and favorable scaling, making it possible to treat relatively large molecules, something that sometimes is infeasible for high-accurate, electron correlation wave function theory (WFT) methods. While its foundations, based on the Hohenberg-Kohn theorems[1] and the Kohn-Sham (KS) equations,[2] are only valid for

ground state properties, Runge and Gross formulated the equivalent of the Hohenberg-Kohn theorems for the description of excited states in 1984,[3] laying the foundations of time-dependent (TD) DFT. For weak external electromagnetic fields, linear-response TD-DFT within the adiabatic approximation[4] has become as important to many different fields working on electronically excited-state problems as DFT is the preferred method for ground state properties.

A ground state DFT calculation precedes the computation of electronic excitation energies within TD-DFT; therefore, both formalisms share the same shortcomings determined by the choice of the underlying density functional approximation (DFA) to the unknown "true" exchange-correlation functional. This work focuses on double-hybrid density functional approximations (DHDFAs) that follow Grimme's definition from 2006,[5] whose outstanding performance have been demonstrated several times for ground state properties, as for example shown in Refs. 6–17. Shortly after the demonstrated success of the first DHDFA B2PLYP[5] for ground state properties, the DHDFA idea was extended to the computation of electronic vertical excitation energies in 2007 when Grimme and Neese[18] combined Head-Gordon's configuration interaction singles with perturbative doubles [CIS(D)][19] approach with the TD-DFT formalism and the closely related Tamm-Dancoff Approximation[20] (TDA). Herein, we exclusively deal with Grimme and Neese's approach, when we use the acronyms TD-DHDFAs and TDA-DHDFAs. We acknowledge other definitions of the DHDFA concept,[9,21–25] but also point out that not all of them are compatible with the TD(A)-DHDFA scheme proposed by Grimme and Neese, which is why they will not be considered in the present work.

Grimme and Neese's first TD(A)-B2PLYP study showed how the inclusion of the perturbative CIS(D) correction reduced the error span by about 0.3 eV compared to the TD(A)-DFT hybrid portion of B2PLYP.[18] That work also showed promising results for singlet-triplet transitions in small (in)organic molecules and for doublet-doublet transitions in small radicals, which were limited to the TDA variant of B2PLYP. Subsequent applications on DHDFAs for excited states involved almost exclusively TD-DHDFA treatments of singlet-singlet transitions in organic systems. In 2009, the TD-DHDFA idea was applied for the first time to B2GP-PLYP[26] on the famous test set containing small organic molecules proposed by Thiel and co-workers,[27] where TD-B2GP-PLYP outperformed TD-B2PLYP and a range of lower-rung DFAs.[28] In 2013, the "non-empirical" functionals PBE0-DH[29] and PBE0-2[30] were also assessed on the same test set in their TDA versions, but it was demonstrated that they were by on average up to 0.08 eV less accurate than TD-B2(GP-)PLYP.[31] Indeed, the label "non-empirical" should not be misunderstood as a synonym for quality or reliability, which was later demonstrated for DHDFAs applied to ground state properties, where semi-empirical DHDFAs by far outperformed non-empirical ones.[10,32] Several studies have been conducted since Grimme and Neese's initial idea, and TD(A)-DHDFAs have been shown to be the most accurate DFAs for excited-state calculations and absorption spectra,[18,28,33–41] even rivaling standard WFT methods.[34,39–41] While we refer the reader to a recently published detailed review on TD(A)-DHDFAs,[42] we highlight only some of the advantages of those over the conventional TD(A)-DFT approaches: a better description of electronic circular dichroism (ECD) spectra,[33] more accurate vertical singlet-singlet[18,28,34,39–43] and singlet-triplet[18,41] excitations in organic molecules—where TD(A)-DHDFAs even outperformed the approximate coupled-cluster singles doubles WFT approach[44,45] [(SCS-)CC2][34]— a more balanced description of the problematic first two excited states in polycyclic aromatic hydrocarbons (PAHs),[35,40] and no misleading results from artificial "ghost states".[28,33,34,36] Another little-known but important finding in the context of ECD spectroscopy is that TD-DHDFAs were the only methods that could successfully reproduce an exciton-coupled spectrum of a merocyanine dimer aggregate,[36] for which even long-range corrected (LC) (or range-separated)

hybrid functionals failed and which initially had only been successfully described with WFT approaches.[46]

A successful strategy to improve DHDFAs for ground state thermochemistry has been the introduction of spin-component and spin-opposite scaling[47–49] (SCS/SOS) to the treatment of the non-local electron-correlation component.[6,11–14,21,50,51] SOS-based methods have the advantage of having a reduced formal scaling behavior if a Laplace transform algorithm is employed.[48,52] We also mention in passing that the currently best-performing DHDFAs for molecular thermochemistry are the SCS-LC-DHDFAs ωDSD$_{72}$-PBEPP86-D4[16] and ωDSD3-PBEPP86-D4[17] based on studies with the GMTKN55[8] database for general main-group thermochemistry, kinetics and noncovalent interactions; however, note that some of these methods follow different strategies compared to Grimme's original DHDFA definition from 2006.

In 2017, significant improvements were achieved by Schwabe and Goerigk when they successfully applied the SCS and SOS techniques to the CIS(D) component[53] of global TD(A)-DHDFAs. A fitting procedure of the SCS/SOS parameters of six global DHDFAs was conducted against a high-level reference data training set. Successful cross-validation studies were carried out for vertical local-valence, vertical Rydberg, and 0-0 singlet-singlet excitations using the TD- and TDA-DHDFA schemes.[39] Scaled and unscaled DHDFAs were again superior to global and LC hybrids.

Their remarkable performance notwithstanding, global TD(A)-DHDFAs suffer from the same flaws as any other global DFA,[40,41,43,54–56] namely the inability to adequately describe charge-transfer (CT) excitations. It was not until recently, in mid-2019, that we closed this gap by introducing the first LC-DHDFAs optimized for vertical singlet-singlet excitation energies, namely TD-ωB2PLYP and TD-ωB2GP-PLYP,[40] both based on the original BLYP-based[57,58] global DHDFAs B2PLYP and B2GP-PLYP, respectively. Therein, we showed how the inclusion of a single parameter, which controls the interplay between the long- and short-range regimes, can improve long-range excitations such as Rydberg states and CT excitations without much loss in accuracy for local-valence transitions. We particularly note that both functionals delivered the best TD-DFT results to date for L_a and L_b transitions in PAHs,[40] and that they have already been successfully used in applications to systems of biological or technological relevance.[59–66]

Prior to mid-2020, most of the BLYP-based global DHDFAs studies had been carried out using the full TD-DHDFA scheme, whereas most of the studies using PBE-based[67] global DHDFAs had used the TDA-DHDFA scheme, instead.[37,38,68–78] Moreover, all previous benchmark studies and applications had been limited to singlet-singlet excitations, except for the original work by Grimme and Neese from 2007,[18] leaving out other spin multiplicities of crucial relevance, such as triplet excitations, most likely due to the lack of a code that could handle those transitions. For this reason, we assessed for the first time singlet-singlet and singlet-triplet excitations with global- and LC-DHDFAs based on both BLYP and PBE expressions for the underlying exchange-correlation functional and compared them with hybrid functionals.[41] Our ωB2(GP-)PLYP and Adamo and co-workers' PBE-QIDH[68] displayed the best results for singlet-triplet excitations, with the latter nevertheless still being unable to properly describe CT excitations, as we had to point out again in 2021.[43] A very important finding was that DHDFAs do not fix the triplet instability problem[79–82] when the full TD-DHDFA scheme is applied, for which the TDA-DHDFA scheme must be employed instead.

Herein, we revisit the idea of applying SCS and SOS techniques to TD(A)-DHDFAs similar to the work done by Schwabe and Goerigk, and we extend them even further by applying the latest TD(A)-LC-DHDFAs not only for singlet-singlet excitations but also to singlet-triplet excitations. For this purpose, we analyze 22 different scaled global- and LC-DHDFAs. Among the 8 unscaled DHDFAs, three are

global and five are LC ones. 6 of those unscaled methods had been analyzed by us before, but we also present two new LC-DHDFAs named ωPBEPP86 and ωB88PP86. The remaining 14 methods are newly developed scaled versions of the 8 unscaled ones. Lastly, we also compare those 22 methods with Mester and Kállay's three newest "Range-Separated Double-Hybrid functional" (RS-DH) methods.[83] The novelty of these RS-DHs is that they have been designed to be long-range corrected not only in the exchange component (as usual LC-methods) but also in the perturbative non-local CIS(D) correction.

In this work, we briefly review the theoretical background required for our new method developments. We then discuss the definition of our new unscaled LC-DHDFAs ωB88PP86 and ωPBEPP86, followed by the development of SCS and SOS extensions for each tested method in this work (except for the RS-DH methods). The new SCS and SOS TD(A)-DHDFAs are then cross-validated in a series of benchmark sets that cover singlet-singlet and singlet-triplet excitations. We finally conclude with a discussion of the general robustness of the newly proposed methods and some final remarks for the user community.

The first version of this manuscript was submitted to this journal on 31 May 2021 and published as a pre-print on ChemRxiv on 1 June.[84] During the peer-review stage of our work, a related article by Mester and Kállay was published in this very same journal.[85] Therein, the authors apply the SCS and SOS ideas to their RS-PBE-P86[83] functional. Those two new functionals differ from our herein proposed methods in two ways. Firstly, they also include range-separation in the CIS(D) part. More importantly, they seem to apply the spin scaling in a slightly different way compared to the established SCS-CIS(D)[53] wave function analogue, contrary to Schwabe and Goerigk's TD(A)-SCS/SOS-DHDFAs[39] and ours. Most cross-validation benchmark sets for SCS/SOS-RS-PBE-P86 are the same as in our present study, which is why we decided to include those new methods in our analysis in this final version of our work. We will show how the conceptually more complicated SCS/SOS-RS-DH approach is not automatically more robust or accurate than our new SCS/SOS methods.

2 Theoretical Background

2.1 Linear-Response TD-DFT

The most common method for computing excited-state properties is linear-response[86–88] time-dependent TD-DFT within the adiabatic approximation.[4,89] The latter allows us to replace the time-dependent exchange-correlation kernel with the time-independent one from ground state DFT. The technicalities of TD-DFT are well-documented in the literature,[18,39,40,76] which is why we keep our explanations as brief as possible. For real orbitals, the vertical excitation energies are computed as the solution of the random-phase-approximation (RPA)-type eigenvalue problem:[90]

$$\begin{pmatrix} \mathbf{A} & \mathbf{B} \\ \mathbf{B} & \mathbf{A} \end{pmatrix} \begin{pmatrix} \mathbf{X}^{(n)} \\ \mathbf{Y}^{(n)} \end{pmatrix} = \Delta E^{(n)} \begin{pmatrix} \mathbf{1} & \mathbf{0} \\ \mathbf{0} & -\mathbf{1} \end{pmatrix} \begin{pmatrix} \mathbf{X}^{(n)} \\ \mathbf{Y}^{(n)} \end{pmatrix}, \quad (1)$$

$\Delta E^{(n)}$ is the vertical excitation energy for the n^{th} excited state, with $\mathbf{X}^{(n)}$ and $\mathbf{Y}^{(n)}$ being the corresponding eigenvectors for single-particle excitations and de-excitations, respectively. $\mathbf{A}$ and $\mathbf{B}$ are matrices that contain the information on these excitations and de-excitations, whose components are given by:[88]

$$\begin{aligned} A_{ia\sigma,jb\tau} = {} & \delta_{\sigma\tau}\delta_{ij}\delta_{ab}(\varepsilon_{a\sigma} - \varepsilon_{i\tau}) + (i_\sigma a_\sigma \mid j_\tau b_\tau) \\ & - \delta_{\sigma\tau} a_x (i_\sigma j_\sigma \mid a_\tau b_\tau) + (1 - a_x)(i_\sigma a_\sigma \mid f^{XC} \mid j_\tau b_\tau) \end{aligned} \quad (2)$$

and

$$\begin{aligned} B_{ia\sigma,jb\tau} = {} & (i_\sigma a_\sigma \mid b_\tau j_\tau) - \delta_{\sigma\tau} a_x (i_\sigma b_\sigma \mid a_\tau j_\tau) \\ & + (1 - a_x)(i_\sigma a_\sigma \mid f^{XC} \mid b_\tau j_\tau) \, . \end{aligned} \quad (3)$$

As usual, σ and τ are spin variables, the indices $i, j, k \ldots$ in this paper refer to occupied orbitals, $a, b, c \ldots$ to virtual orbitals, and a_X is the Fock exchange scaling parameter. The last term in these equations has DFT origin, where f^{XC} is the exchange-correlation kernel and defined as the second derivative of the exchange-

correlation functional E_{XC} with respect to the electronic density ρ:

$$f^{XC}(\mathbf{r}_1, \mathbf{r}_2) = \frac{\partial^2 E_{XC}}{\partial\rho(\mathbf{r}_1)\partial\rho(\mathbf{r}_2)} \tag{4}$$

with $\mathbf{r}_{1/2}$ being spatial variables.

By neglecting the **B** matrix from Eq.(1), we can obtain a simplified version known as the Tamm-Dancoff approximation (TDA),[20] resulting in an eigenvalue problem that reads

$$\mathbf{AX}^{(n)} = \Delta E^{(n)}\mathbf{X}^{(n)}. \tag{5}$$

The label (n) will be dropped in the following.

2.2 Vertical Excitation Energies with DHDFAs

We follow Grimme's original definition of DHDFAs[18] alongside the LC scheme,[91] similar as in our construction of ωB2(GP-)PLYP:[40]

$$\begin{aligned} E_{XC}^{LC\text{–}DHDFA} = {} & a_X E_X^{SR\text{–}HF}(\omega) + a_{X,DFA} E_X^{SR\text{–}DFT}(\omega) \\ & + E_X^{LR\text{–}HF}(\omega) + a_{C,DFA} E_C^{DFT} + a_C E_C^{PT2}, \end{aligned} \tag{6}$$

where the first term corresponds to short-range Fock exchange, followed by the short-range DFT-exchange functional. The third term is the full, long-range Fock exchange to ensure the correct $1/r_{12}$ decay in the potential, where r_{12} is the interelectronic distance. The last two terms are the DFT-correlation functional and the second-order perturbative, non-local-correlation correction given by MP2[92] for ground state or CIS(D) for excitation energy calculations. Finally, $a_{X,DFA}$ and $a_{C,DFA}$ are scaling parameters for DFT exchange and correlation, whereas a_X and a_C scale short-range Fock exchange and non-local correlation, respectively; usually, but not always, those parameter values depend on one another.[5,29,31,68,93] The interplay between short- and long-range regimes is controlled by the range-separation parameter ω.

In the spirit of ground state DHDFA calculations, Grimme and Neese's vertical excitation energies at the double-hybrid level ($\Delta E_{TD(A)\text{–}DHDFA}$) are obtained in a two-step procedure;[18] first, we solve either the full TD-(Eq.1) or TDA-DFT (Eq.5) eigenvalue problem using only the hybrid part of the DHDFA, i.e., all terms in Eq. 6 excluding the perturbative portion. This gives rise to a vertical excitation energy of hybrid-DFT quality ($\Delta E_{TD(A)\text{–}hybrid}$), which is then perturbatively corrected with Head-Gordon's CIS(D) correction ($\Delta_{CIS(D)}$):[19]

$$\Delta E_{TD(A)\text{–}DHDFA} = \Delta E_{TD(A)\text{–}hybrid} + a_C \Delta_{CIS(D)}, \tag{7}$$

where the parameter a_C scales the CIS(D)-type contribution. More details on TD(A)-DHDFAs are given in our recent free-access account in Ref. 42.

2.3 The CIS(D) Correction

The CIS(D) formalism for TD(A)-DHDFAs has been extensively explained in the literature and we refer the reader to Refs 18 and 39 for more detailed information. In the spirit of MP2 being a second-order perturbative correlation correction to a Hartree-Fock (HF) ground state energy, the second-order perturbative CIS(D) correction[19] introduces some electron correlation to configuration interaction singles (CIS) excitation energies. The CIS(D) energy correction to the total CIS energy of an excited state is:

$$E_C^{CIS(D)} = \langle\Phi_{CIS}|\hat{V}|\hat{U}_2\Phi_0\rangle + \langle\Phi_{CIS}|\hat{V}|\hat{T}_2\hat{U}_1\Phi_0\rangle, \tag{8}$$

where the first and second terms are known as the "direct" and "indirect" terms, respectively. $\hat{U}_1$ and $\hat{U}_2$ are operators that generate the singly- and doubly-excited wave functions from the HF determinant (Φ_0), $\hat{T}_2$ is the operator that generates the double excitation of two CIS-inactive electrons, and $\hat{V}$ is a perturbation potential. Φ_{CIS} is the CIS wave function according to:

$$\Phi_{CIS} = \hat{U}_1\Phi_0 = \sum_{ia} t_i^a \Phi_i^a, \tag{9}$$

where t_i^a are the CIS single-excitation amplitudes and Φ_i^a is the singly excited determinant. The $\hat{T}_2$ operator acting on the HF determinant, Φ_0, is given by

$$\begin{aligned}\hat{T}_2\Phi_0 &= \frac{1}{4}\sum_{ijab} t_{ij}^{ab}\Phi_{ij}^{ab} \\ &= -\frac{1}{4}\sum_{ijab}\frac{(ij||ab)}{\varepsilon_a+\varepsilon_b-\varepsilon_i-\varepsilon_j}\Phi_{ij}^{ab},\end{aligned} \tag{10}$$

where we have used Mulliken's notation for the antisymmetrized two-electron integral $(ij \,||\, ab) = (ij \mid ab) - (ia \mid jb)$ and ε stands again for the orbital energy. Φ_{ij}^{ab} is the doubly-excited determinant from the HF ground state created by the operator $\hat{U}_2$:

$$\hat{U}_2\Phi_0 = -\frac{1}{4}\sum_{ijab}\frac{\langle\Phi_{ij}^{ab}|\hat{V}|\hat{U}_1\Phi_0\rangle}{\varepsilon_a+\varepsilon_b-\varepsilon_i-\varepsilon_j-\Delta E_{CIS}}\Phi_{ij}^{ab} \tag{11}$$

The actual CIS(D) correction, $\Delta_{CIS(D)}$, to the CIS excitation energy, ΔE_{CIS}, is obtained as the difference between the second-order perturbative correlation energies for the excited and the ground states:

$$\begin{aligned}\Delta_{CIS(D)} &= E_C^{CIS(D)} - E_C^{MP2} \\ &= -\frac{1}{4}\sum_{ijab}\frac{(u_{ij}^{ab})^2}{\varepsilon_a+\varepsilon_b-\varepsilon_i-\varepsilon_j-\Delta E_{CIS}} + \sum_{ia} t_i^a v_i^a,\end{aligned} \tag{12}$$

with the corresponding definitions

$$u_{ij}^{ab} = \sum_c (ab \,||\, cj)t_i^c - (ab \,||\, ci)t_j^c - \sum_k (ka \,||\, ij)t_k^b - (kb \,||\, ij)t_k^a \tag{13}$$

and

$$v_i^a = \frac{1}{2}\sum_{jkbc}(jk \,||\, bc)[t_i^b t_{jk}^{ca} + t_j^a t_{ik}^{cb} + 2t_j^b t_{ik}^{ac}] \tag{14}$$

A TD(A)-DHDFA excitation energy is calculated by employing Eq.12 with KS orbitals instead of the HF ones and with $\Delta E_{TD(A)\text{–hybrid}}$ excitation energies instead of ΔE_{CIS}. For TDA-DHDFA, it is straightforward to employ the $\mathbf{X}$ vector (Eq.5) for the single-excitation amplitudes t_i^a, whereas for the full TD-DHDFA the $\mathbf{X}$ vector is employed but the $\mathbf{Y}$ vector neglected (Eq.1).

2.4 The SCS- and SOS-CIS(D) Variants

Similar to Grimme's SCS-MP2 method,[47] the electron pair contributions to the correlation energy of an excitation energy can be separated into same (SS) and opposite spin (OS) contributions, which are then scaled differently . The first implementation of the SCS-CIS(D) idea dates back to 2004 when Grimme and Izgorodina applied the same scaling parameters as in SCS-MP2 ground state theory to the "indirect" term in Eq. 8.[94] Later, Rhee and Head-Gordon extended this idea and applied additional scale parameters to the "direct" term.[53] Therefore, we can break down the two terms in Eq.(8) into same- and opposite spin components according to:

$$\begin{aligned}E_c^{SCS-CIS(D)} &= \left\langle\Phi_{CIS} \mid \hat{V} \mid \left(c_U^{OS}\hat{U}_2^{OS} + c_U^{SS}\hat{U}_2^{SS}\right)\Phi_0\right\rangle \\ &+ \left\langle\Phi_{CIS} \mid \hat{V} \mid \left(c_T^{OS}\hat{T}_2^{OS} + c_T^{SS}\hat{T}_2^{SS}\right)\hat{U}_1\Phi_0\right\rangle,\end{aligned} \tag{15}$$

where c_U^{SS} and c_U^{OS} are the same- and opposite-spin scale parameters for the direct term and c_T^{SS} and c_T^{OS} the related parameters for the indirect term. We refer the reader to e.g. Ref. 39 for the explicit form of the SS and OS terms shown in Eq.(15). By setting the SS parameters to zero, one reduces the SCS- to the SOS-CIS(D) approach, which can benefit from a better formal scaling behavior in the same way as SOS-MP2.[48] Note that the individual scaling of the direct and indirect terms has been shown to be beneficial as opposed to an SCS-CIS(D) variant that applied the same SS and OS parameters to both terms.[34]

Coming back to TD(A)-DHDFs, the expression for the SCS/SOS-CIS(D) correction ($\Delta_{SCS/SOS\text{–}CIS(D)}$), which is added to the excitation energy of the hybrid portion of the DHDFA, follows the same structure as $\Delta_{CIS(D)}$ in Eq.(7), once the four SS/OS terms are taken into consideration, giving the TD(A)-SCS/SOS-DHDF excitation energy:

$$\Delta E_{TD(A)\text{–}SCS/SOS\text{–}DHDFA} = \Delta E_{TD(A)\text{–}hybrid} + \Delta_{SCS/SOS\text{–}CIS(D)}. \tag{16}$$

Note that in the work by Rhee and Head-Gordon, the definition of the $U_2^{SS/OS}$ operator considers an extra "damping" parameter (λ)

for ΔE_{CIS} and two different versions of SCS-CIS(D) were developed by setting λ=0 and λ=1. Herein, we set this parameter to unity following the same protocol as in Refs 34 and 39.

As this final version of our study now also includes the new SCS/SOS-RS-PBE-P86 methods,[85] we would like to point out that theoretical details on those are not clear regarding the application of SCS/SOS to the CIS(D) part. As the authors did not acknowledge Rhee and Head-Gordon's SCS-CIS(D) approach and did not use the phrases "direct" and "indirect" term, it is safe to assume that both terms were subjected to the same scaling parameters. Moreover, the same two SS and OS scaling parameters were applied to both the SR and LR part of their CIS(D) implementation.

3 Computational Details

All molecular geometries were taken from the literature, and all calculations were performed with the same AO basis set used in the respective works that developed the reference values to enable a direct comparison. In this context, we refrain from any basis set dependence study as it has already been conducted.[39] It has been established that even for full CIS(D) (a_C=1), local-valence and Rydberg excitation energies only differed by about 0.03 eV when going from a triple to a large quadruple-ζ basis set. Unsurprisingly, this difference was even lower for DHDFAs with smaller a_C. For instance, there was an average difference of just 0.01 eV for TD-B2PLYP (a_C=0.27) and TD-PBE0-DH (a_C=0.125).[39] We implemented the SCS/SOS-CIS(D) code for singlet and triplet excitations into a local version of the ORCA code,[95–97] and it has just become available for free in ORCA5. The SCF convergence criterion was set to $10^{-7}E_h$ ($10^{-8}E_h$ for the updated Gordon set) along with ORCA's numerical quadrature grid "4" (grid "5" and "finalgrid 6" for the updated Gordon set). The resolution-of-the-identity technique was used with appropriate auxiliary basis sets for the perturbative steps.[98,99]

Hybrid density functionals are not assessed in this work because we aim to improve our previously published DHDFA results by introducing two new exchange-correlation combinations and also the SCS/SOS technique. We refer the reader to our previous works in Refs. 40 and 41 for more information about the performance of global and LC hybrid functionals, which are shown to be less accurate and robust; in this context, we would just like to mention that the LC hybrid ωB97X[100] sometimes outperformed some DHDFAs such as B2PLYP,[5] PBE0-DH,[29] and RSX-QIDH,[101] but not other DHDFAs tested by us. Due to a lack of high-level reference data for triplet excitations in the PAH and CT sets, we expand our analysis by also assessing the full TD-DHDFA scheme on these two sets without any further optimization procedure. In addition, we also assessed the new (SCS/SOS-)RS-DH methods by Mester and Kállay,[83,85] namely, RS-B88-LYP, RS-PBE-PBE, RS-PBE-P86, and SCS/SOS-RS-PBE-P86 which had been optimized with Schwabe and Goerigk's "updated Gordon set"[39,102] for singlet-singlet transitions using the TDA-DHDFA scheme; note that for these methods, we took the relevant values directly from the original works. Singlet-triplet excitations have only been assessed with (SCS/SOS)-RS-PBE-P86 in Ref. 85 and we could not find data for the other two RS-DHs.

It is also important to consider the definition of "chemical accuracy" for excitation energy calculations. It is a somewhat arbitrarily defined value and some studies have suggested a value of 0.05 eV,[70,103] whereas others prefer to regard an accuracy of 0.1 eV as a success.[28,104] Our study can be interpreted within the context of either of these two definitions.

Table 1: Optimized parameters for our new LC-DHDFAs following Eq. 6.

Functional	a_X	$a_{X,DFA}$	$a_{C,DFA}$	a_C	ω[bohrs^{-1}]
ωB88PP86	0.65	0.35	0.58	0.42	0.20
ωPBEPP86	0.70	0.30	0.68	0.48	0.18

4 Development

4.1 Introducing ωB88PP86 and ωPBEPP86

Our new ωB88PP86 and ωPBEPP86 functionals are based on Becke88 and PBE exchange, respectively, however with modifications proposed by Hirao and co-workers[91] in order to make them applicable within the LC scheme. Both methods rely on Perdew's correlation functional from 1986 (P86)[105] with the Vosko, Wilk, and Nusair "VWN-V" local spin-density component.[106] The choice of those exchange and correlation functionals is based on the good performance of the global PBE-based DHDFA from our previous study,[41] namely PBE-QIDH, where it was able to properly describe Rydberg transitions, the RS-PBE-P86 method that performed well for the updated Gordon test set,[83] and the DSD-PBEP86[12] ground state DHDFA that performed well for ground state thermochemistry[8] and some excited-state properties.[39]

Both methods follow the LC-DHDFA definition from Eq.6 and were optimized for singlet-singlet excitations, using the TDA-DHDFA scheme, by minimizing the root-mean-square deviation (RMSD) for the well-balanced updated Gordon set. We performed the optimization for singlet-singlet excitations using only the TDA-DHDFA scheme due to its more affordable computational cost and to make them applicable to singlet-triplet excitations, based on our previous experience with TDA- and TD-DHDFAs.[41] We optimized these methods only for singlet-singlet transitions to make them comparable to previously published methods. The original benchmark set by Gordon and co-workers[102] comprised a total of 63 vertical singlet-singlet excitations made up of 32 valence and 31 Rydberg states in 14 different molecules but was based on different types of geometries and experimental reference values. Schwabe and Goerigk re-optimized the geometries with a consistent level of theory in 2017,[39] and also provided new full and estimated Approximate Coupled-Cluster Singles Doubles Triples data (CC3[107]/aug-cc-pVTZ[108,109]).

For the optimization procedure of ωB88PP86 and ωPBEPP86, we set the initial scaling parameters for the DFT, Fock exchange, and perturbative correlation components to those of B2GP-PLYP and PBE-QIDH, respectively. Those starting parameters were chosen, as both functionals performed reasonably well for local-valence excitations. We then optimized ω. Finally, a "full" optimization of all remaining scale parameters was carried out for that ω value, giving rise to the final values presented in Table 1.

Interestingly, our resulting scale parameters for Fock exchange and perturbative correlation follow Toulouse *et al.'s* one-parameter quadratic relation ($a_X^2 = a_C$),[93] even though the latter had not been derived for excitation energies. Results for the new methods for the fit set will be discussed further below after the introduction of the new SCS/SOS methods.

4.2 New TDA-DHDFAs with SCS and SOS Components for Excitation Energies

4.2.1 Fitting Procedure

We combined the TD(A)-DHDFA idea with the SCS/SOS-CIS(D) approach as presented earlier in Eq. 16. For that purpose, we considered eight different unscaled DHDFA methods: B2PLYP,[5] B2GP-PLYP,[26] ωB2PLYP,[40] ωB2GP-PLYP,[40] PBE-QIDH,[68] RSX-QIDH,[101] ωB88PP86, and ωPBEPP86. According to our previous work in Ref. 41, PBE0-DH and RSX-0DH[110] do not perform well, particularly the latter, which is why we refrained from including them in this work. Since SCS and SOS variants of B2PLYP and B2GP-PLYP have already been presented in Ref. 39, we will label our new variants as SCS/SOS-B2PLYP21 and SCS/SOS-B2GP-PLYP21, respectively. We re-optimized these two DHDFAs given that this time we also include singlet-triplet excitations in the fitting procedure (see below). For each one of these functionals, we analyzed two different flavors for the scaling parameters:

- A free fit of all four parameters (SCS variant).
- An SOS variant with $c_T^{SS} = c_U^{SS} = 0$ and a free fit of the remaining two OS parameters.

On rare occasions, the free fit of the four parameters gave negative, unphysical values for one or both SS parameters. In those cases, we set those parameters to zero. In two cases, namely B2PLYP and ωB2PLYP, the SCS fit led to the SOS variant. Hence, the subsequently used label "SCS/SOS-B2PLYP21" refers to one and the same method; the same is true for "SCS/SOS-ωB2PLYP.

The fitting procedure was conducted with the full updated Gordon benchmark set. This includes the 63 vertical singlet-singlet excitations mentioned in Section 4.1 and additional data for singlet-triplet excitations developed as part of Ref. 39 and published for the first time by us in mid-2020.[41] Those 38 vertical singlet-triplet excitations are made up of 27 valence and 11 Rydberg excitations from 12 different molecules, all with the same full or estimated high-level CC3/aug-cc-pVTZ reference data.

Our parametrization procedure consisted of a minimization of the RMSD for each method on the entire set. The final optimized scaling parameters are shown in Table 2. Therein, we also provide a breakdown into which DHDFAs are global and which are long-range corrected. We analyze the singlet-singlet and singlet-triplet excitation energies for the fit set separately in the following two sections.

Table 2: Original[a] parameters of unscaled DHDFAs and parameters of their new SCS and SOS variants optimized for the TDA-DHDFA scheme.

Method		c_T^{SS}	c_T^{OS}	c_U^{SS}	c_U^{OS}
B2PLYP[b]	Original	0.270	0.270	0.270	0.270
	SCS[c]	0.000	0.334	0.000	0.283
	SOS[c]	0.000	0.334	0.000	0.283
B2GP-PLYP[b]	Original	0.360	0.360	0.360	0.360
	SCS	0.018	0.475	0.000	0.468
	SOS	0.000	0.489	0.000	0.484
PBE-QIDH[b]	Original	0.330	0.330	0.330	0.330
	SCS	0.070	0.515	0.096	0.524
	SOS	0.000	0.547	0.000	0.573
ωB2PLYP[d]	Original	0.270	0.270	0.270	0.270
	SCS[c]	0.000	0.433	0.000	0.460
	SOS[c]	0.000	0.433	0.000	0.460
ωB2GP-PLYP[d]	Original	0.360	0.360	0.360	0.360
	SCS	0.000	0.571	0.135	0.558
	SOS	0.000	0.570	0.000	0.610
RSX-QIDH[d]	Original	0.330	0.330	0.330	0.330
	SCS	0.174	0.541	0.586	0.424
	SOS[e]	0.000	0.632	0.000	0.714
ωB88PP86[d]	Original	0.423	0.423	0.423	0.423
	SCS	0.000	0.557	0.092	0.545
	SOS	0.000	0.559	0.000	0.599
ωPBEPP86[d]	Original	0.480	0.480	0.480	0.480
	SCS	0.000	0.610	0.297	0.540
	SOS	0.000	0.613	0.000	0.669

[a] If all four scaling parameters are identical, the original, unscaled DHDF is obtained, as all parameters equal a_C in Eq. 7. [b] Global DHDFA. [c] The SCS fitting procedure led directly to the SOS parameters (see main text). [d] LC-DHDFA. [e] Not to be confused with the ground-state optimized SOS-RSX-PBE-QIDH published while this manuscript was under review.[111]

4.2.2 Analysis of Vertical Singlet-Singlet Excitations

Our results for the singlet excitations in the fit sets are broken down into the whole set and its local-valence and Rydberg components. All relevant statistical results are shown in Table 3 for each TDA-DHDFA method. First of all, we would like to point out that many methods share the same RMSDs. However, to be able to rank them, we decided to sort the methods according to the following criteria: RMSD, MAD, MD, and error span(Δ_{err}). For example, PBE-QIDH's SCS and SOS variants have identical RMSDs, MADs, and MDs and differ only in the error span. In this case, the SCS variant occupies a higher place in the ranking given its lower error span (0.78 vs. 0.81 eV). Most of the time these differences are negligible, but we decided to apply the same criteria throughout the present work to be consistent.

We note that the introduction of the SCS/SOS scheme is overall beneficial for each of our own methods when considering the statistics for the entire set of singlet-singlet excitations. Most methods display large reductions of their RMSD for both local-valence and Rydberg excitations upon introduction. For instance, the RMSD for RSX-QIDH for the complete set is reduced from 0.40 eV to 0.21/0.24 eV for its SCS/SOS variants, respectively. This coincides with a reduction of 0.25 eV in the RMSD for local-valence excitations for both the SCS and SOS methods, and a reduction of 0.10/0.04 eV for SCS/SOS for the Rydberg excitations. Some other methods, on the other hand, have an overall improved RMSD despite not improving for both local-valence and Rydberg excita-

Table 3: Statistical values (in eV) for all, local-valence, and Rydberg singlet-singlet excitations in the updated Gordon set using the TDA-DHDFA formalism.[a]

	Overall				Local-valence				Rydberg			
Method	MD	MAD	RMSD	Δ_{err}	MD	MAD	RMSD	Δ_{err}	MD	MAD	RMSD	Δ_{err}
SCS-PBE-QIDH	0.07	0.12	0.16	0.78	0.13	0.14	0.18	0.48	0.01	0.11	0.13	0.54
SOS-PBE-QIDH	0.07	0.12	0.16	0.81	0.12	0.13	0.17	0.53	0.02	0.12	0.14	0.54
SCS-ωPBEPP86	0.07	0.14	0.17	0.82	0.09	0.12	0.16	0.51	0.04	0.15	0.17	0.69
SOS-ωB88PP86	0.05	0.14	0.18	0.94	0.11	0.13	0.17	0.54	0.00	0.16	0.19	0.79
SCS-RS-PBE-P86	0.06	0.13	0.19	0.91	0.14	0.17	0.22	0.84	–0.02	0.09	0.14	0.80
SCS-ωB88PP86	0.08	0.15	0.19	0.95	0.15	0.16	0.19	0.53	0.01	0.15	0.18	0.77
SOS-ωPBEPP86	0.10	0.16	0.19	0.81	0.10	0.13	0.19	0.57	0.10	0.18	0.20	0.73
RS-PBE-P86	0.04	0.14	0.20	0.88	0.13	0.18	0.24	0.86	–0.05	0.10	0.14	0.72
SCS-ωB2GP-PLYP	0.04	0.14	0.20	1.10	0.13	0.15	0.20	0.67	–0.07	0.13	0.19	0.77
SOS-RS-PBE-P86	0.09	0.15	0.20	0.98	0.14	0.17	0.23	0.87	0.04	0.14	0.18	0.95
PBE-QIDH	0.12	0.15	0.20	0.75	0.23	0.23	0.27	0.49	0.01	0.08	0.10	0.47
RS-PBE-PBE	0.03	0.15	0.20	0.91	0.13	0.18	0.24	0.91	–0.07	0.11	0.15	0.73
ωB88PP86	0.06	0.16	0.21	1.00	0.15	0.15	0.21	0.50	–0.04	0.16	0.21	0.85
SOS-ωB2GP-PLYP	0.06	0.16	0.21	1.11	0.15	0.17	0.23	0.70	–0.04	0.14	0.19	0.79
SCS-RSX-QIDH	0.12	0.17	0.21	0.83	0.14	0.15	0.21	0.57	0.10	0.19	0.21	0.73
RS-B88-LYP	–0.02	0.18	0.22	1.00	0.11	0.18	0.24	0.97	–0.16	0.18	0.20	0.72
SCS/SOS-ωB2PLYP	0.07	0.17	0.22	1.18	0.17	0.19	0.24	0.66	–0.03	0.16	0.21	0.93
ωPBEPP86	0.13	0.18	0.22	0.94	0.17	0.17	0.23	0.58	0.08	0.19	0.22	0.80
SOS-B2GP-PLYP21	–0.03	0.19	0.22	1.01	0.15	0.16	0.19	0.51	–0.21	0.21	0.24	0.51
SCS-B2GP-PLYP21	0.01	0.19	0.22	1.00	0.19	0.20	0.23	0.50	–0.19	0.19	0.22	0.52
SOS-RSX-QIDH	0.12	0.20	0.24	0.83	0.08	0.16	0.21	0.64	0.16	0.24	0.27	0.80
ωB2GP-PLYP	0.12	0.19	0.25	1.08	0.26	0.26	0.32	0.65	–0.03	0.11	0.15	0.73
ωB2PLYP	0.12	0.20	0.26	1.14	0.26	0.26	0.32	0.62	–0.03	0.14	0.18	0.89
B2GP-PLYP	–0.13	0.24	0.28	1.10	0.06	0.14	0.19	0.70	–0.33	0.33	0.36	0.57
SCS/SOS-B2PLYP21	–0.02	0.25	0.29	1.22	0.23	0.23	0.27	0.64	–0.27	0.27	0.30	0.54
RSX-QIDH	0.35	0.35	0.40	0.89	0.41	0.41	0.46	0.79	0.28	0.28	0.31	0.60
B2PLYP	–0.29	0.34	0.41	1.33	–0.09	0.18	0.24	0.96	–0.50	0.50	0.53	0.70

[a] The aug-cc-pVTZ AO basis set was used in all cases. The DHDFAs are sorted by their overall RMSDs. The values for the (SCS/SOS-)RS-DH methods were taken from Refs 83 and 85. The statistical estimators are Mean Deviation(MD), Mean-Absolute Deviation (MAD), Root-Mean-Square Deviation (RMSD), and Error Span (Δ_{err}).

tions. For example, for B2PLYP the RMSD for local-valence excitations slightly increases from 0.24 to 0.27 eV for its SCS/SOS variant. This is accompanied by a considerable reduction in the RMSD for the Rydberg excitations (from 0.53 to 0.30 eV), which leads to a reduction of the overall RMSD from 0.41 to 0.29 eV. We see something similar for PBE-QIDH were an improvement in the local-valence category compensated for slightly increased RMSDs for Rydberg states when SCS/SOS is applied.

An exception to the above said seems to be SCS-RS-PBE-P86. SCS only shows a marginal improvement of 0.01 eV in the RMSD compared to RS-PBE-P86. SOS induces no change to the RMSD but a by 0.1 eV larger error span. ωPBEPP86, which contains the same underlying DFT components as RS-PBE-P86, benefits from both SOS (RMSD reduced by 0.03 eV) and SCS (RMSD reduced by 0.05 eV). MDs and error spans also improve for SCS/SOS-ωPBEPP86.

When ranking all assessed methods according to their results for the entire set of singlet-singlet excitations, we find that PBE-QIDH's SCS and SOS variants yield the lowest RMSDs with 0.16 eV in both cases, closely followed by SCS-ωPBEPP86, SOS-ωB88PP86, SCS-RS-PBE-P86, SCS-ωB88PP86, and SOS-ωPBEPP86. These seven methods are the only ones with RMSDs below 0.2 eV. We also identify five methods that share an RMSD of exactly 0.20 eV, namely, RS-PBE-P86, SCS-ωB2GP-PLYP, SOS-RS-PBE-P86, PBE-QIDH, and RS-PBE-PBE. It is noteworthy that the new RS-DHs, along with PBE-QIDH, still perform well despite being unscaled methods. In the same context, another well-performing unscaled DHDFA is ωB88PP86, which has the same RMSD of 0.21 eV as SOS-ωB2GP-PLYP and SCS-RSX-QIDH. Five DHDFAs immediately follow, all with the same RMSD of 0.22 eV, i.e., RS-B88-LYP, SCS/SOS-ωB2PLYP, ωPBEPP86, SOS- and SCS-B2GP-PLYP21. The remaining five DHDFAs with values below 0.3 eV are SOS-RSX-QIDH, the unscaled ωB2GP-PLYP, the related ωB2PLYP, B2GP-PLYP , and finally SCS/SOS-B2PLYP21. Lastly, RSX-QIDH and B2PLYP are the two worst performers for this set with RMSDs of 0.40 and 0.41 eV.

The MADs follow more or less the same trends as the RMSDs. It is remarkable that the SCS and SOS versions of PBE-QIDH, ωB88PP86, and ωPBEPP86 are very close to the second definition of "chemical accuracy" for

excited states, i.e., with average absolute deviations of up to 0.1 eV. On the other hand, the MDs show an interesting behavior once the SCS/SOS schemes are applied. Most of the tested unscaled methods, regardless of systematic over or underestimation of the excitation energies, show a systematic improvement by having MDs that are closer to zero. For instance, RSX-QIDH overestimates the energies by on average 0.35 eV, which is improved by the SCS and SOS variants with MD = 0.12 eV in both cases. B2PLYP tends to underestimate the excitation energies (MD=–0.29 eV), whereas the SCS/SOS-B2PLYP21 variant has one of the best MDs with a value of only –0.02 eV. Some unscaled DHDFAs with very good MDs that we would like to highlight are the three new RS-DH methods (MDs range from 0.04 to –0.02 eV) and ωB88PP86 (MD=0.06 eV).

When focussing just on local-valence transitions, we observe similar trends as before. The best performer is SCS-ωPBEPP86 with RMSD=0.16 eV, which is closely followed by SOS-ωB88PP86 and PBE-QIDH's SOS and SCS variants. Other good performers below 0.2 eV are SOS-ωPBEPP86, B2GP-PLYP and its SOS version, and SCS-ωB88PP86. The majority of the remaining methods display results between 0.2 eV and 0.3 eV, except for ωB2PLYP, ωB2GP-PLYP (both with RMSDs of 0.32 eV), and RSX-QIDH (0.46 eV).

We end the discussion of singlet excitations by analyzing the Rydberg category. The unscaled PBE-QIDH functional is the best performer with an excellent value of 0.10 eV. What is surprising is the fact that its SCS and SOS variants display slightly larger RMSDs of 0.13 eV and 0.14 eV, respectively. However, as we mentioned before, this mishap is greatly compensated for by its reduction of about 0.10 eV in the local-valence category. The SCS-RS-PBE-P86 method has a value of 0.14 eV and occupies the third place in the ranking, followed by RS-PBE-P86, ωB2GP-PLYP, and RS-PBE-PBE with RMSDs of 0.15 eV. The next DHDFAs in our ranking are SCS-ωPBEPP86, ωB2PLYP, SOS-RS-PBE-P86, SCS- and SOS-ωB2GP-PLYP, and SOS-ωB88PP86. The remaining methods have RMSDs between 0.20 eV (RS-B88-LYP and SOS-ωPBEPP86) and 0.53 eV (B2PLYP).

4.2.3 Analysis of Vertical Singlet-Triplet Excitations

Following the same idea as presented by us in Ref. 41, we perform two different analyses for singlet-triplet excitations. The first type covers all transitions between the ground state singlet to the various triplet excited states, which we denote as S0-TN, with N $\geq$ 1. The second type focuses on the energy splitting between the first singlet and triplet excited states, denoted as S1-T1. The latter is particularly intriguing for potential future applications of well-performing methods in areas such as singlet-fission materials.[112–116] It also gives us first insights into the robustness of a method, as there is no guarantee that a method that performs well for singlet excitations is also suitable for triplet ones.

All Singlet-Triplet Excitations in this set (S0-TN)

In Table 4, we see that nearly every tested TDA-DHDFA seems to describe singlet-triplet excitations with a very good or acceptable RMSD below 0.2 eV, except for B2GP-PLYP (0.22 eV) and B2PLYP (0.34 eV). PBE-QIDH and its SCS/SOS variants perform outstandingly well, with RMSDs below the second definition of "chemical accuracy" for excitation energies, with values of 0.08-0.09 eV. Just a few hundredths of an eV above, we locate SCS-RS-PBE-P86, RS-PBE-P86, SCS-ωB88PP86, the unscaled ωPBEPP86, and SOS-ωPBEPP86, which are closely followed by SOS-ωB2GP-PLYP, SOS-ωB88PP86, and the unscaled ωB2GP-PLYP (RMSD = 0.13 eV). We then find that ten DHDFAs, both scaled and unscaled ones, present good values between 0.14 and 0.15 eV, and based on our other criteria outlined earlier we rank them from ωB88PP86 to SCS-RSX-QIDH. Interestingly, RSX-QIDH and SCS/SOS-B2PLYP21 deliver acceptable results below 0.20 eV. We also notice that, in general, most unscaled TDA-DHDFAs are slightly outperformed by their corresponding

Table 4: Statistical values (in eV) for the S0-TN transitions in the updated Gordon set using the TDA-DHDFA formalism.[a]

	Overall				Local-valence				Rydberg			
Method	MD	MAD	RMSD	Δ_{err}	MD	MAD	RMSD	Δ_{err}	MD	MAD	RMSD	Δ_{err}
SCS-PBE-QIDH	–0.04	0.06	0.08	0.31	–0.04	0.06	0.08	0.30	–0.04	0.08	0.10	0.30
SOS-PBE-QIDH	–0.04	0.07	0.08	0.33	–0.04	0.06	0.08	0.31	–0.03	0.08	0.10	0.33
PBE-QIDH	–0.04	0.07	0.09	0.37	–0.04	0.08	0.10	0.37	–0.04	0.05	0.06	0.15
SCS-RS-PBE-P86	0.02	0.09	0.10	0.37	0.04	0.10	0.11	0.37	–0.04	0.07	0.08	0.19
RS-PBE-P86	–0.01	0.09	0.11	0.36	0.01	0.10	0.11	0.36	–0.08	0.08	0.10	0.18
SCS-ωB88PP86	–0.07	0.09	0.12	0.40	–0.06	0.08	0.10	0.37	–0.09	0.12	0.15	0.40
ωPBEPP86	0.00	0.10	0.12	0.37	0.01	0.08	0.10	0.33	–0.04	0.14	0.14	0.37
SOS-ωPBEPP86	–0.05	0.10	0.12	0.47	–0.08	0.09	0.11	0.35	0.02	0.11	0.13	0.42
SOS-ωB2GP-PLYP	–0.05	0.10	0.13	0.60	–0.02	0.09	0.10	0.48	–0.13	0.14	0.18	0.41
SOS-ωB88PP86	–0.09	0.10	0.13	0.43	–0.08	0.09	0.11	0.37	–0.10	0.14	0.17	0.43
ωB2GP-PLYP	–0.02	0.11	0.13	0.58	0.02	0.10	0.12	0.51	–0.13	0.13	0.15	0.28
ωB88PP86	–0.07	0.11	0.14	0.45	–0.03	0.08	0.10	0.34	–0.17	0.18	0.22	0.38
SCS-ωB2GP-PLYP	–0.08	0.11	0.14	0.56	–0.05	0.09	0.11	0.45	–0.16	0.16	0.21	0.40
SOS-RS-PBE-P86	0.08	0.12	0.14	0.45	0.10	0.12	0.15	0.37	0.02	0.10	0.12	0.33
SCS-ωPBEPP86	–0.09	0.12	0.14	0.44	–0.12	0.12	0.14	0.30	–0.03	0.11	0.12	0.36
SOS-B2GP-PLYP21	–0.04	0.11	0.15	0.64	0.03	0.07	0.09	0.41	–0.22	0.22	0.23	0.28
SCS/SOS-ωB2PLYP	–0.08	0.11	0.15	0.62	–0.04	0.09	0.11	0.48	–0.16	0.17	0.22	0.49
SCS-B2GP-PLYP21	–0.01	0.12	0.15	0.65	0.06	0.09	0.11	0.43	–0.19	0.19	0.21	0.28
ωB2PLYP	–0.06	0.12	0.15	0.61	–0.02	0.10	0.12	0.51	–0.16	0.16	0.19	0.38
SOS-RSX-QIDH	–0.07	0.13	0.15	0.57	–0.12	0.13	0.15	0.36	0.04	0.14	0.16	0.49
SCS-RSX-QIDH	–0.10	0.13	0.15	0.49	–0.14	0.14	0.15	0.29	–0.02	0.12	0.13	0.35
RSX-QIDH	0.06	0.15	0.17	0.57	0.01	0.13	0.16	0.57	0.18	0.18	0.20	0.22
SCS/SOS-B2PLYP21	–0.02	0.16	0.19	0.71	0.09	0.11	0.13	0.42	–0.28	0.28	0.30	0.32
B2GP-PLYP	–0.13	0.16	0.22	0.62	–0.03	0.07	0.10	0.35	–0.37	0.37	0.38	0.27
B2PLYP	–0.24	0.26	0.34	0.87	–0.11	0.14	0.17	0.45	–0.56	0.56	0.57	0.39

[a] The aug-cc-pVTZ AO basis set was used in all cases. The DHDFAs are sorted by their overall RMSDs. The values for the (SCS/SOS-)RS-DH methods were taken from Refs 83 and 85. The statistical estimators are Mean Deviation(MD), Mean-Absolute Deviation (MAD), Root-Mean-Square Deviation (RMSD), and Error Span (Δ_{err}).

SCS/SOS variants.

The MDs display small underestimations with absolute MDs below 0.1 eV, except for B2PLYP (–0.24 eV) and B2GP-PLYP (–0.13 eV). We point out that the only DHDFAs that display slight overestimations are SCS-RS-PBE-P86 (0.02 eV), RSX-QIDH (0.06 eV), and SOS-RS-PBE-P86 (0.08 eV). In general, inclusion of SCS/SOS seems to keep the MDs nearly unchanged, such as in PBE-QIDH, or it produces a slight red shift, such as in ωPBEPP86 (see Table 4.2.3)

S1-T1 Analysis

In Table 5, we see that the statistics for the S1-T1 splitting show similar trends as for the S0-TN analysis with most RMSDs being below 0.2 eV. In the updated Gordon set, most low-lying excitation energies belong to the local-valence category, and only for the water molecule we have to analyze a Rydberg excitation.

RS-PBE-P86's SCS and SOS variants, and B2GP-PLYP's SOS and SCS variants are at the top of the ranking with RMSDs ranging from 0.07 to 0.09 eV. PBE-QIDH's SCS and SOS variants, and ωB2GP-PLYP's SCS and SOS variants also display the same outstanding result with RMSD = 0.1 eV. Ten methods follow closely ranging from the unscaled RS-PBE-P86 (0.11 eV) to the scaled SCS-ωPBEPP86 (0.15 eV). Other acceptably well-performing DHDFAs are B2PLYP, ωB2GP-PLYP, SOS-RSX-QIDH, and PBE-QIDH, and ωB2PLYP. Finally, SCS-RSX-QIDH and its unscaled variant conclude the list with values of 0.22 and 0.33 eV, respectively.

One major difference to the previous S0-TN analysis is the fact that the MDs are mostly positive, with only two exceptions (SOS-RS-PBE-P86 and B2PLYP). The reason is simply that most DHDFAs display a systematic overestimation for singlet-singlet excitations, whereas they systematically underestimate singlet-triplet excitations. As a result, it is expected that the S1-T1 energy splitting also displays an overestimation.[41]

Our findings for the updated Gordon set are very promising. Our new SCS/SOS variants show considerable improvements over their unscaled parents for singlet-singlet transitions, while for singlet-triplet excitations there is a more modest improvement. In sections 5 and 6 we will further discuss how our new methods perform in an extensive cross-validation study that covers both singlet-singlet and singlet-triplet excitations, including CT excitations, which have not been part of our parameter training.

Table 5: Statistical values (in eV) for the S1-T1 energy splitting on the updated Gordon set using the TDA-DHDFA formalism.[a]

Method	MD	MAD	RMSD	Δ_{err}
SCS-RS-PBE-P86	0.05	0.06	0.07	0.18
SOS-RS-PBE-P86	−0.02	0.05	0.08	0.33
SOS-B2GP-PLYP21	0.02	0.07	0.08	0.26
SCS-B2GP-PLYP21	0.03	0.08	0.09	0.29
SOS-PBE-QIDH	0.07	0.09	0.10	0.26
SOS-ωB2GP-PLYP	0.07	0.09	0.10	0.26
SCS-ωB2GP-PLYP	0.08	0.09	0.10	0.24
SCS-PBE-QIDH	0.08	0.09	0.10	0.23
RS-PBE-P86	0.08	0.08	0.11	0.28
B2GP-PLYP	0.01	0.10	0.12	0.40
ωPBEPP86	0.09	0.11	0.13	0.28
SCS/SOS-ωB2PLYP	0.10	0.12	0.13	0.27
SOS-ωB88PP86	0.10	0.12	0.13	0.35
ωB88PP86	0.11	0.12	0.14	0.33
SCS-ωB88PP86	0.11	0.13	0.15	0.33
SCS/SOS-B2PLYP21	0.04	0.12	0.15	0.47
SOS-ωPBEPP86	0.09	0.11	0.15	0.44
SCS-ωPBEPP86	0.11	0.13	0.15	0.38
B2PLYP	−0.03	0.13	0.16	0.50
ωB2GP-PLYP	0.14	0.15	0.18	0.41
SOS-RSX-QIDH	0.11	0.13	0.19	0.54
PBE-QIDH	0.16	0.16	0.19	0.41
ωB2PLYP	0.16	0.17	0.20	0.44
SCS-RSX-QIDH	0.18	0.18	0.22	0.42
RSX-QIDH	0.28	0.28	0.33	0.56

[a] The aug-cc-pVTZ AO basis set was used in all cases. The DHDFAs are sorted by their overall RMSDs. The values for the (SCS/SOS-)RS-DH methods were taken from Refs 83 and 85. The statistical estimators are Mean Deviation(MD), Mean-Absolute Deviation (MAD), Root-Mean-Square Deviation (RMSD), and Error Span (Δ_{err}).

5 Cross-Validation for Vertical Singlet-Singlet Excitations

5.1 The ωB2(GP-)PLYP Training Set

The ωB2(GP-)PLYP "training set"[40] is a slight modification of the original set used by Schwabe and Goerigk for their parametrization of TD(A)-SCS/SOS-DHDFAs in 2017.[39] It contains 34 vertical singlet-singlet excitations, made of up 28 valence and 6 Rydberg transitions. The reference values are based on Coupled Cluster Singles Doubles with Perturbative Triples Excitation Correction[117] [CCSDR(3)] with the large aug-cc-pVTZ AO basis set. Note that herein we do not use this set for any fitting procedure but called it "training set" to indicate that it was used during the development of our ωB2(GP-)PLYP functionals.[40] We present the RMSD, MAD, and MD values for our herein assessed TDA-DHDFAs in Fig. 1, where the results are, once again, broken down into local-valence and Rydberg transitions. The methods are sorted according to their RMSD values for the overall set, which are also shown on top of the bars. All raw as well as other statistical data are provided in the Supporting Information (SI). We note in passing that the "top 10" methods are SCS/SOS variants, with the RS-DH methods coming right after them. Indeed, the RS-DH methods have previously been among the most accurate DHDFAs in Ref. 83 and it was argued that it was due to range-separation in the perturbative CIS(D) treatment. We show here nevertheless that even better results can be achieved through the SCS/SOS technique without the need of introducing range-separation in the perturbative treatment. This is an encouraging outcome and a strong indicator that the SCS/SOS methods can be transferred to systems other than the ones used in the fit. We now proceed with the analysis of the RMSDs for this set.

PBE-QIDH's SOS and SCS variants and SCS-RS-PBE-P86 are at the top of the ranking with equal RMSDs of 0.12 eV, but are closely followed by SCS-ωPBEPP86 and SOS-RS-PBE-P86 with just one-hundredth of an eV above the former three. Next, ωB88PP86's SCS and SOS variants along with SCS-ωB2GP-PLYP display the same RMSD, followed by a group of five methods all with identical RMSDs: SOS-ωPBEPP86, SOS-ωB2GP-PLYP, SOS-B2GP-PLYP21, SCS-RSX-QIDH, and RS-B88-LYP. RS-PBE-PBE and RS-PBE-P86 are placed slightly above those (RMSD = 0.17 eV) and they are followed by SCS/SOS-ωB2PLYP, ωPBEPP86, and SCS-B2GP-PLYP21 (RMSD = 0.18 eV). The remaining two DHDFAs below an RMSD of 0.2 eV are ωB88PP86 and SOS-RSX-QIDH. Thus, we have identified a total of 18 methods that yield RMSDs below 0.2 eV most of which are SCS or SOS variants, with SCS/SOS-B2PLYP21 being the only exception (RMSD=0.26 eV). All remaining methods have RMSDs that range from 0.20 eV (PBE-QIDH) to 0.36 eV (RSX-QIDH).

Our new SCS and SOS variants also display improvements when just analyzing local-valence transitions. We briefly summarize that there are four methods that occupy the first position in the ranking and also fulfill the second

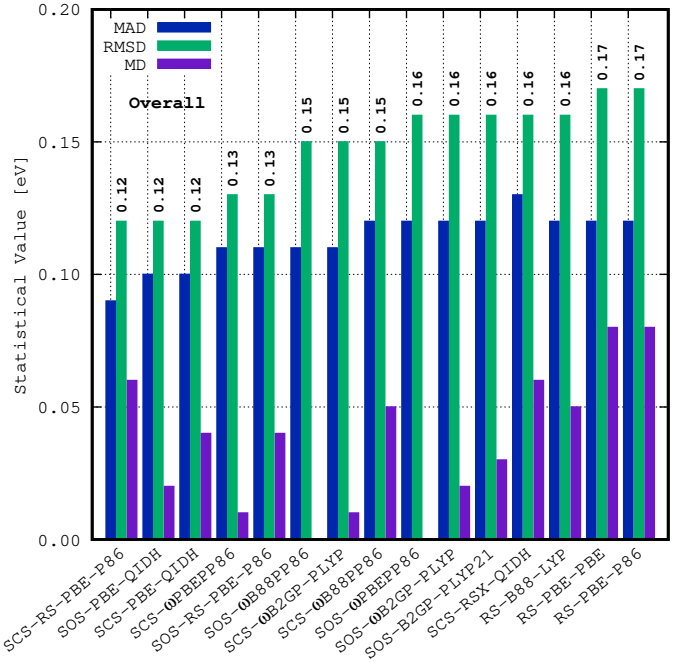

Figure 1: Statistical values (in eV) for the complete ωB2(GP-)PLYP training set, namely RMSDs (values shown over each bar), MADs, and MDs. Only the best 15 methods are shown; values for all assessed methods and a breakdown of the statistics into local-valence and Rydberg excitations can be found in the SI. The values for the (SCS/SOS-)RS-DH methods were taken from Refs 83 and 85. The aug-cc-pVTZ AO basis set was used in all cases.

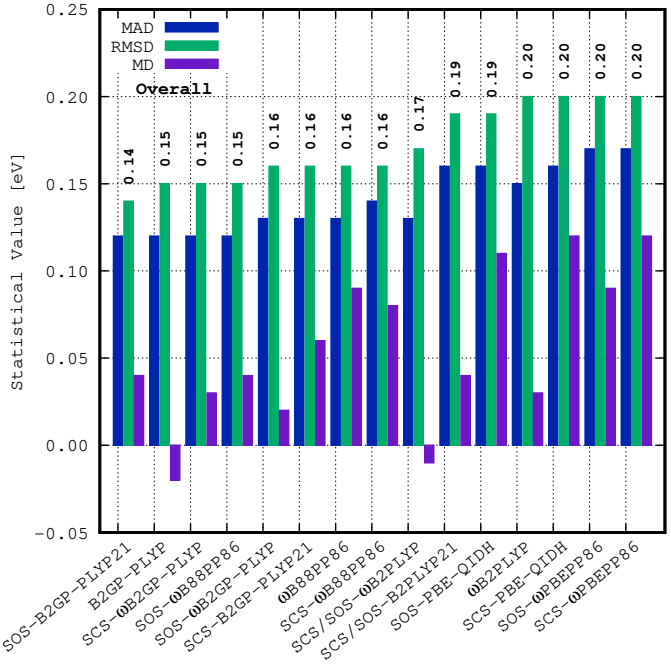

Figure 2: Statistical values (in eV) for the complete Loos and Jacquemin set, namely RMSDs (values shown over each bar), MADs, and MDs. Only the best 15 methods are shown; values for all assessed methods and a breakdown of the statistics into local-valence and Rydberg excitations can be found in the SI. The aug-cc-pVTZ AO basis set was used in all cases.

definition of "chemical accuracy" given above, namely, SOS-ωB88PP86, SOS-PBE-QIDH, and ωB2GP-PLYP's SCS and SOS variants with RMSDs of 0.10 eV. Almost every SCS and SOS method is ranked in the best places and performs better than its unscaled parent, except for SCS-B2GP-PLYP21 and SCS/SOS-B2PLYP21. For Rydberg transitions, some of the SCS and SOS variants have slightly increased RMSDs compared to their unscaled parents. PBE-QIDH is such an example where the RMSD increases by 0.04 and 0.06 eV when the SCS and SOS formalisms are applied.

In the following sections, we will test our new methods on more challenging systems where unscaled DHDFAs have presented problems in the past.[40,41,83]

5.2 The Loos and Jacquemin Benchmark Set

We also analyzed the systems introduced by Loos, Jacquemin, and co-workers in their 2018 benchmark set.[118] However, similarly to our previous works,[40,41] and due to overlap with already tested systems, we only consider 29 of their excitations divided into 16 valence and 13 Rydberg transitions in 11 different systems, namely acetaldehyde, acetylene, carbon monoxide, diazomethane, dinitrogen, hydrogen chloride, hydrogen sulfide, ketene, methanimine, nitrosomethane, and thioformaldehyde. All reference values have CC3/aug-cc-pVTZ quality. All statistical results are shown in Fig. 2. It is worthwhile to point out that the analysis of this set in Refs 83 and 85 did not avoid such duplication of excitations, which might artificially increase the reported total number of assessed excitations.

Note that amongst the top 15 we mostly find our new SCS/SOS methods, whereas the RS-DH and SCS/SOS-DH methods are not featured (Fig. 2). The best RMSD for this set is obtained with SOS-B2GP-PLYP21 (0.14 eV), closely followed by the unscaled B2GP-PLYP, SCS-ωB2GP-PLYP, and SOS-ωB88PP86 (RMSD = 0.15 eV in each case). We also highlight SOS-ωB2GP-PLYP, SCS-B2GP-PLYP21, ωB88PP86, and SCS-ωB88PP86

(RMSD = 0.16 eV in each case). The last three methods with an RMSD below 0.2 eV are SCS/SOS-ωB2PLYP, SCS/SOS-B2PLYP21 and SOS-PBE-QIDH. The four DHDFAs with RMSDs of exactly 0.2 eV are ωB2PLYP, SCS-PBE-QIDH, and ωPBEPP86's SCS and SOS variants. Most of the remaining methods with RMSDs above 0.2 eV are unscaled DHDFAs, such as ωB2GP-PLYP, the five (SCS/SOS-)RS-DH methods, or PBE-QIDH. That being said, we find that RSX-QIDH's SCS and SOS variants also belong to this range. The unscaled RSX-QIDH yields the highest RMSD of 0.38 eV, confirming other studies that this LC-DHDFA is often less accurate than its global PBE-QIDH counterpart.[32,41]

When focussing solely on local-valence excitations, we notice similar trends as for the two previously discussed sets with most of the SCS and SOS variants being positioned at the top and RMSDs ranging from 0.13 eV (SOS-PBE-QIDH and SOS-ωPBEPP86) to 0.16 eV (SOS-RSX-QIDH, SCS-RS-PBE-P86, SCS-ωB2GP-PLYP, and ωB88PP86). Note that the unscaled RS-DH methods perform equally well with RMSDs of 0.16-0.17 eV, values that they share with B2PLYP, B2GP-PLYP, SCS-RSX-QIDH, SOS-B2GP-PLYP21, SOS-RS-PBE-P86, and SOS-ωB2GP-PLYP. The last two methods with RMSDs below 0.2 eV are ωPBEPP86 and SCS-B2GP-PLYP21 (0.18 eV). All remaining methods have RMSDs above 0.20 eV.

As we already pointed out in Ref. 40, we called this set *the difficult cases set* because its Rydberg states do not seem to require the LC scheme, contrary to the examples discussed earlier. Note that this trend is also seen for all SCS/SOS-)RS-DH methods, which show large blue-shifts for this category (MDs of 0.23, 0.29, 0.28, 0.30 eV for RS-B88-LYP, SOS-RS-PBE-P86, RS-PBE-PBE, SCS-RS-PBE-P86 and RS-PBE-P86, respectively) Hence, it is not surprising that the two top places in our ranking are global DHDFAs methods (SOS-B2GP-PLYP21 and SCS/SOS-B2PLYP21). However, our new SCS- and SOS-LC-DHDFAs improve over their unscaled parents and yield more accurate results, for instance, SCS/SOS-ωB2PLYP and ωB2PLYP (0.12 vs. 0.14 eV), SCS-ωB2GP-PLYP and ωB2GP-PLYP (0.14 vs. 0.20 eV).

In summary, our SCS/SOS variants of global and LC-DHDFAs are the best-performing methods even for the *difficult cases* presented by Loos, Jacquemin, and co-workers. None of these systems were assessed in the previous sets, demonstrating that our new methods are robust enough, even for the treatment of challenging systems like the ones discussed in this section.

5.3 The "Exotic-Molecules" Set

In mid-2020, Loos and Jacquemin *et al.* presented a new benchmark set under the name "exotic molecules set". With that name the authors intended to imply that each of the molecules in this set includes at least one atom representing elements that is uncommon in usual organic-molecule test sets, namely: F, Cl, Si, or P.[119] The overall set comprises 19 local-valence singlet-singlet excitations from 14 different systems with high-level CC3/aug-cc-pVTZ reference values. We remind the reader that the inclusion of these "exotic molecules" made the TD-DHDFA scheme unable to correctly describe these kind of systems and better results were obtained with the TDA-DHDFA formalism, as we thoroughly discussed in Ref. 41. Therefore, the user might take this into consideration when the system under study presents any of the aforementioned species.

Based on the RMSDs presented in Fig. 3, the unscaled RS-DH methods yield the lowest RMSDs (< 0.1 eV), which is an outstanding finding. B2GP-PLYP and SCS-RS-PBE-P86 also display excellent values of exactly 0.10 eV for this test set, closely followed by our new ωPBEPP86 (0.12 eV), SCS-PBE-QIDH (0.13 eV). Our new SCS and SOS methods feature in the ranking from this point onward, with B2PLYP, SOS-RS-PBE-P86, SCS-ωPBEPP86, and SCS-RSX-QIDH being the first ones with good values of 0.13 eV. 14 other methods, all of which developed for this study, have RMSDs that range from 0.14 to 0.18 eV . Lastly, SOS-RSX-QIDH and its parent RSX-QIDH are placed in last position with RMSDs of 0.20 and 0.22 eV. respectively. We conclude that al-

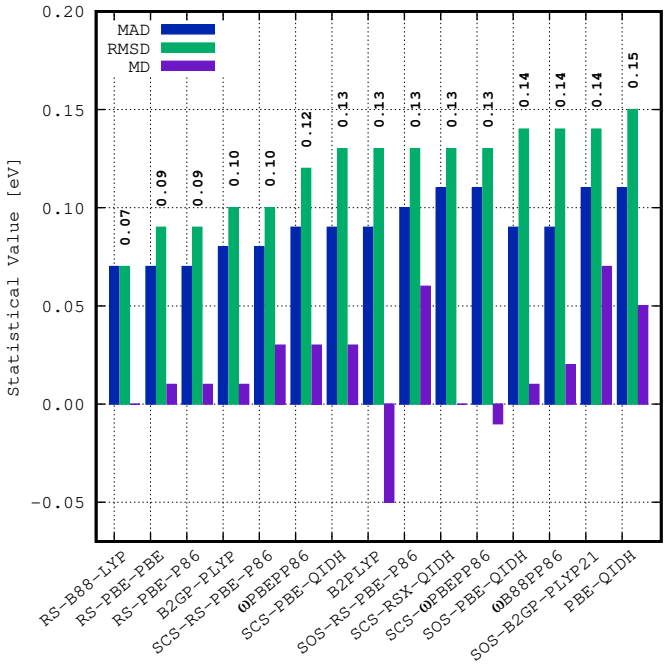

Figure 3: Statistical values (in eV) for the "exotic-molecules" set, namely RMSDs (values shown over each bar), MADs, and MDs. Only the best 15 methods are shown; values for all assessed methods can be found in the SI. The values for the (SCS/SOS-)RS-DH methods were taken from Refs 83 and 85. The aug-cc-pVTZ AO basis set was used in all cases.

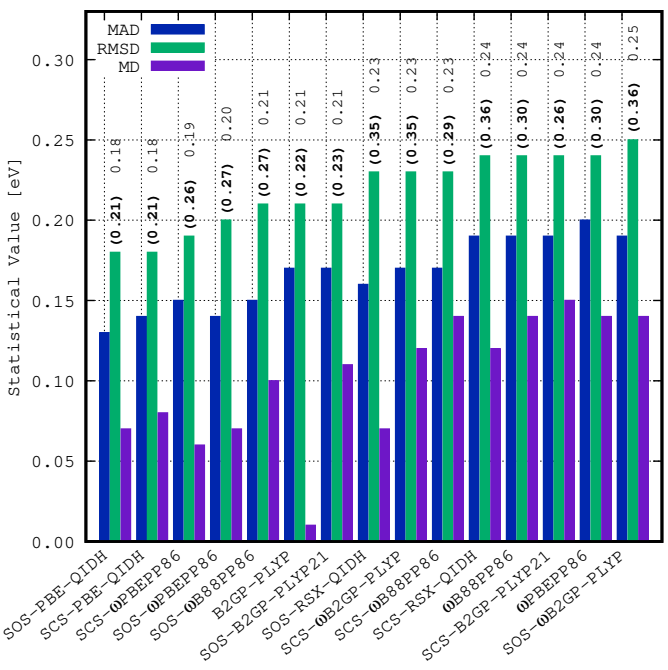

Figure 4: Statistical values (in eV) for the Thiel set, namely RMSDs (values shown over each bar), MADs, and MDs. Values in parentheses are RMSDs after including the 2^1A_g state in octatetraene. Only the best 15 methods are shown; values for all assessed methods can be found in the SI. The TZVP AO basis set was used in all cases.

most every assessed method performs fairly well compared to the previous sets given that their RMSDs mostly lie below 0.20 eV.

In general, the MDs are well-balanced for this set, regardless of the use of SCS or SOS. Except for SCS/SOS-B2PLYP21 and SCS-B2GP-PLYP21 (MDs=0.15 eV), and SOS-RSX-QIDH (MD=–0.10 eV), every other method has absolute MDs below 0.1 eV.

5.4 The Thiel Benchmark Set

To keep investigating our new SCS/SOS methods' capabilities a bit further, we also analyze parts of the popular benchmark set introduced by Thiel and co-workers.[27] The original set comprises 167 valence excitations, 104 of which are singlet-singlet excitations with various WFT reference values, out of which we chose the CC3/TZVP[120] ones in agreement with previous works in Refs 39,41. Therein, we outlined why we refrain from using Thiel and co-workers' CAS-PT2[121] references. We consider CC3 as one of the currently best single-reference approaches for excitation energies. If less-expensive, single-reference TDA-DHDFAs results approach CC3 quality, this constitutes a major advancement.[39,41]

In order to avoid duplication with previous sets, we only analyze 36 local-valence singlet excitations from 8 different systems, namely: acetamide, benzoquinone, imidazole, norbornadiene, octatetraene, propanamide, pyridazine, and pyrimidine. Again, duplication of systems and excitations has not been avoided in Refs 83 and 85 (see similar comment in Section 5.2)

This test set differs from previous ones given the large RMSDs for every tested method. After a closer inspection, we found that the 2^1A_g state in octatetraene displays a very large overestimation, reaching more than 1 eV in some cases. In 2011, Angeli and Pastore[122] considered octatetraene as a somewhat complicated system due to its high double-excitation character. Previous work on TD-B2(GP-)PLYP also showed this state to be problematic.[28] In light of this finding, we report the statistical results by considering and excluding this state, where the former case is shown in parentheses (Fig. 4).

When considering all excitations, PBE-QIDH's SCS and SOS variants are in the lead, closely followed by the unscaled B2GP-PLYP and its SOS variant, all of them with RMSDs slightly above 0.2 eV. Seven DHDFAs have RMSDs between 0.26 and 0.29 eV; with the exception of PBE-QIDH, all methods have been newly developed for this study. ωB88PP86 and ωPBEPP86 have RMSDs of exactly 0.30 eV. Six methods yield high RMSDs that range from 0.33 to 0.36 eV, namely, B2PLYP, SCS/SOS-ωB2PLYP, RSX-QIDH's SCS and SOS variants, and ωB2GP-PLYP's SCS and SOS variants. Finally, the unscaled RS-DHs and ωB2PLYP have values of 0.40 eV, whereas SCS-RS-PBE-P86,SCS-RS-PBE-P86, ωB2GP-PLYP and RSX-QIDH come last with RMSDs of 0.41, 0.43, 0.43, and 0.54 eV, respectively.

When excluding the 2^1A_g state in octatetraene, the ranking of methods changes. Now, most of the SCS and SOS variants are placed at the top except for SCS/SOS-PBE-P86. Compared to the analysis in the previous paragraph, those methods with the highest RMSDs benefit from a large reduction (on average 0.1 eV), whereas the ones with the low RMSDs benefit from a smaller reduction (on average 0.05 eV). The three best performers this time are PBE-QIDH's SCS and SOS variants and SCS-ωPBEPP86 with RMSDs below 0.2 eV. We also see improvements for various methods after excluding the 2^1A_g state in octatetraene, with reductions in the RMSDs of up to 0.13 eV, such as SCS-ωB2GP-PLYP, SCS/SOS-ωB2PLYP, or the five (SCS/SOS-)RS-DH methods. They now all perform similarly to unscaled PBE-QIDH. Lastly, the unscaled B2PLYP, ωB2PLYP, and ωB2GP-PLYP also have improved values (RMSD = 0.33 eV in each case), whereas RSX-QIDH is still in last place with a value of 0.45 eV. Overall, we can conclude that most SCS/SOS variants show superior performance for a set that seems to be challenging to describe.

5.5 ^1L_a and ^1L_b Transitions in Linear Polycyclic Aromatic Hydrocarbons

Linear polycyclic aromatic hydrocarbons (PAHs) have gained particular interest due to their possible applications in light-emitting diodes or photovoltaics, to name two examples. According to the Platt nomenclature, the two lowest singlet-singlet excitations are usually called ^1L_a and ^1L_b.[123] The former exhibits a polarization along the short axis of the molecule, whereas the second is polarized along the long axis.[124] It has also been suggested that the ^1L_a state has ionic character, while the ^1L_b state has covalent character.[125–127] Conventional TD-DFT fails to describe both states with comparable accuracy; as shown in detail in Refs 35,124 and 40, a good description of one state comes at the cost of the other. In summary, LC-hybrid functionals provide a better description of ^1L_a excitations, but they tend to overestimate the ^1L_b ones.[35,128] In 2011, it was shown for the first time that global TD-DHDFAs partially solved this problem compared to CC2 reference data.[35] In 2019, we confirmed this finding once again when we analyzed the same 5 linear systems (from naphthalene to hexacene) with our new TD-LC-DHDFAs[40] but, in contrast to the 2011 work, we relied on high-level CR-EOM-CCSD(T)[129] data as well as the experimental reference values taken from Ref. 124. We found that ωB2GP-PLYP was the best TD-DFT method at that time with results that were slightly better than CC2.[40] Herein, we re-analyze the same five systems with the same high-level reference values. All calculations were performed with the cc-pVTZ AO basis set. Due to the lack of high-level reference data for triplet excitations in this test set, we present results not only using the TDA-DHDFA scheme but also for the full TD-DHDFA scheme, as no triplet-instability problems are expected. This allows us also to test the transferability of our SCS/SOS parameters to the full TD-DHDF scheme.

Regarding the energy splitting between the two states we see an improvement when

Table 6: Statistical results (in eV) for the ^1L_a–^1L_b energy gap over the five linear polyacenes from naphthalene to hexacene using TDA (left) and full TD algorithms (right).[a]

	TDA-DHDFA					TD-DHDFA			
Method	MD	MAD	RMSD	Δ_{err}	Method	MD	MAD	RMSD	Δ_{err}
SOS-RSX-QIDH[b]	–0.03	0.03	0.03	0.01	SCS-ωB2GP-PLYP	–0.02	0.03	0.03	0.08
SOS-ωB2GP-PLYP	–0.08	0.08	0.08	0.05	SOS-ωPBEPP86	0.03	0.03	0.04	0.06
SOS-ωPBEPP86[b]	–0.08	0.08	0.08	0.02	SOS-ωB2GP-PLYP[b]	0.02	0.03	0.04	0.09
SOS-ωB88PP86	–0.10	0.10	0.10	0.04	SOS-ωB88PP86	–0.04	0.04	0.04	0.06
SCS-ωB2GP-PLYP	–0.11	0.11	0.11	0.03	SCS-ωPBEPP86	–0.07	0.07	0.07	0.05
SCS/SOS-ωB2PLYP	–0.12	0.12	0.13	0.07	SOS-PBE-QIDH	–0.08	0.08	0.08	0.02
SOS-PBE-QIDH	–0.13	0.13	0.13	0.02	SCS-ωB88PP86[b]	–0.09	0.09	0.09	0.05
SOS-RS-PBE-P86	0.05	0.13	0.14	0.38	SOS-RS-PBE-P86[c]	–	–	–	–
SCS-ωB88PP86	–0.14	0.14	0.14	0.04	SCS/SOS-ωB2PLYP[b]	–0.09	0.09	0.10	0.09
SCS-RS-PBE-P86	–0.13	0.13	0.16	0.24	SCS-RS-PBE-P86[c]	–	–	–	–
SOS-B2GP-PLYP21	–0.17	0.17	0.17	0.04	SCS-RSX-QIDH	–0.13	0.13	0.13	0.03
SCS-ωPBEPP86	–0.17	0.17	0.17	0.01	SOS-RSX-QIDH	0.14	0.14	0.14	0.09
SCS-PBE-QIDH	–0.18	0.18	0.18	0.02	SCS-PBE-QIDH	–0.14	0.14	0.14	0.02
SCS-B2GP-PLYP21	–0.18	0.18	0.19	0.04	SOS-B2GP-PLYP21	–0.19	0.19	0.19	0.02
RS-B88-LYP	–0.23	0.23	0.24	0.19	SCS-B2GP-PLYP21	–0.21	0.21	0.21	0.01
RS-PBE-PBE	–0.23	0.23	0.24	0.20	ωPBEPP86	–0.23	0.23	0.23	0.05
RS-PBE-P86	–0.23	0.23	0.24	0.20	ωB88PP86	–0.26	0.26	0.26	0.03
SCS-RSX-QIDH	–0.25	0.25	0.25	0.05	ωB2GP-PLYP	–0.27	0.27	0.27	0.02
ωPBEPP86	–0.26	0.26	0.26	0.05	RSX-QIDH	–0.31	0.31	0.31	0.03
ωB88PP86	–0.27	0.27	0.27	0.03	ωB2PLYP	–0.32	0.32	0.32	0.04
ωB2GP-PLYP	–0.28	0.28	0.28	0.01	B2GP-PLYP	–0.35	0.35	0.35	0.05
ωB2PLYP	–0.28	0.28	0.28	0.05	PBE-QIDH	–0.38	0.38	0.38	0.04
SCS/SOS-B2PLYP21	–0.29	0.29	0.29	0.07	SCS/SOS-B2PLYP21	–0.43	0.43	0.43	0.01
RSX-QIDH	–0.31	0.31	0.31	0.02	B2PLYP	–0.44	0.44	0.44	0.03
B2GP-PLYP	–0.33	0.33	0.33	0.04	RS-B88-LYP[c]	–	–	–	–
PBE-QIDH	–0.36	0.36	0.36	0.03	RS-PBE-PBE[c]	–	–	–	–
B2PLYP	–0.36	0.36	0.36	0.03	RS-PBE-P86[c]	–	–	–	–

[a] All calculations were performed with the cc-pVTZ AO basis set. The values for the (SCS/SOS-)RS-DH methods were taken from Refs 83 and 85. [b] These methods perform well for each one of the ^1L_a and ^1L_b states, as well as for the energy splitting. [c] TD-DHDFA data not available.

SCS/SOS is applied, however, there are two potential reasons for this observation: (a) either both the ^1L_a and ^1L_b excitations improve and, therefore, the energy gap between them also agrees better with the reference, or (b) the excitations to both states are shifted similarly but their energy difference matches with the reference. Ideally, the situation described in (a) is more desirable than (b), however, the energy differences also provide information that is as important and valuable as the values for the individual states. Those methods that belong to the situation described in (a) are highlighted in footnote b in Table 6, where we present the statistics for the energy gap over the five systems. The complete raw data and the statistics for each of the ^1L_a and ^1L_b states can be found in the SI.

Similar to previous test sets, most of our SCS/SOS variants occupy the best positions in the ranking, with the exception of SCS-RSX-QIDH and SCS/SOS-B2PLYP21. For the TDA-DHDFA scheme, we identify one and three methods that fulfill the first and second definition of "chemical accuracy", respectively, namely SOS-RSX-QIDH (RMSD = 0.03 eV), SOS-ωB2GP-PLYP (RMSD = 0.08 eV), SOS-ωPBEPP86 (RMSD = 0.08 eV), and SOS-ωB88PP86 (RMSD = 0.10 eV). Amongst those four methods, which all display outstanding results, we highlight SOS-RSX-QIDH and SOS-ωPBEPP86 as functionals that satisfy the situation described in (a), i.e., the simultaneous improvement of both types of excitations. Ten other methods follow with RMSDs below 0.2 eV, the best of which are SCS-ωB2GP-PLYP, SCS/SOS-ωB2PLYP, SOS-PBE-QIDH, SOS-RS-PBE-P86, and SCS-ωB88PP86. The three RS-DH methods share an RMSD of 0.24 eV, followed by SCS-RSX-QIDH with a value of 0.25 eV. Next, we find the unscaled methods ωPBEPP86, ωB88PP86 , ωB2GP-PLYP, ωB2PLYP, and SCS/SCS-B2PLYP21, all of which are the remaining methods with RMSDs below 0.3 eV.

For the TD-DHDFA scheme, the picture is not too different, since most of the SCS/SOS methods are at the top of the ranking, with SCS/SOS-B2PLYP21 being the only exception. It is noteworthy that we now see eight methods that fulfill the second definition of "chemical accuracy", of which the best-four methods also fulfill the first definition (see Table 6); these are: SCS-ωB2GP-PLYP, SOS-ωPBEPP86, SOS-ωB2GP-PLYP, and SOS-ωB88PP86, SCS-ωPBEPP86 , SOS-PBE-QIDH, SCS-

ωB88PP86 , and finally SCS/SOS-ωB2PLYP. Among those methods, SOS-ωB2GP-PLYP, SCS-ωB88PP86, and SCS/SOS-ωB2PLYP belong to category (a). Interestingly, SCS-RSX-QIDH follows this time with a good RMSD of 0.13 eV, closely followed by its SOS variant and SCS-PBE-QIDH. SOS-B2GP-PLYP21 is the last method with an RMSD below 0.2 eV. Similarly to the TDA-DHDFA analysis, ωPBEPP86, ωB88PP86, and ωB2GP-PLYP display RMSDs above 0.2 eV. The remaining unscaled methods and SCS/SOS-B2PLYP21 yield RMSDs above 0.3 eV.

Regarding the correct energy order of the states, only a few methods give the wrong order for anthracene with respect to the experimental data, where the ^1L_a–^1L_b experimental gap is –0.04 eV. For the TDA-DHDFA scheme, only five methods fail, namely, SOS-ωB2GP-PLYP (gap of 0.01 eV), SOS-RSX-QIDH (0.06 eV), SOS-ωPBEPP86 (0.01 eV), SCS-RS-PBE-P86 (0.01 eV), and SOS-RS-PBE-P86 (0.22 eV). For the TD-DHDFA scheme, seven methods fail in this regard: SCS- and SOS-ωB2GP-PLYP (0.06 and 0.10 eV, respectively), SOS-PBE-QIDH (0.01 eV), SOS-RSX-QIDH (0.21 eV), SOS-ωB88PP86 (0.04 eV), SCS- and SOS-ωPBEPP86 (0.01 and 0.11 eV, respectively). Note that the CR-EOM-CCSD(T) method also yields the wrong order of states for anthracene (0.10 eV) compared to experimental data.

In summary, to the best of our knowledge the results for some of the new methods developed herein constitute the best TD(A)-DFT results published to date for these systems.

5.6 An Update on Charge-Transfer Excitations

The LC methods were mainly developed with the aim to solve the charge-transfer (CT) problem of TD-DFT, and we proceed with a full assessment of our "updated" CT set presented in Ref. 40. In 2020, we modified this set and here we use the same systems again. Those are: 2,4-dichloro-6-p-N,N-diethylaminobiphenylyl-1,3,5-triazine (DBQ),[34] para-nitroaniline (pNA),[130] dimethylaminobenonitrile (DMABN),[130] benzene-tetracyanoethylene complex (B-TCNE),[130] hydrogen chloride (HCl),[118] a dipeptide,[131] a β-dipeptide,[131] and finally N-phenylpyrrole (PP).[132] Similar to the previous set, we also present full TD-DHDFA results due to the lack of data for singlet-triplet excitations. The high-level reference data used in this set are: theoretically back-corrected from the experiment (DBQ), linear-response CCSDR(3) (pNA and peptides), EOM-CCSD(T) (DMABN and B-TCNE), and linear-response CC3 (HCl), respectively (also see SI). Note that most of our CT systems were recently updated by Loos, Jacquemin and co-workers in Ref. 133. However, we used our reference values already presented in Refs. 40 and 41 to be consistent with those studies and the basis sets employed therein and for those reference values.

When inspecting Table 7, it should not come as a surprise that global TD(A)-DHDFAs are not suitable for describing CT excitations. We point out that the opposite has been claimed in 2020[76] but disproven by us on three occasions.[40,41,43] This study constitutes the fourth occasion. As already discussed by us for aryl-TCNE complexes,[43] we observe again that global DHDFAs artificially benefit from the TDA-DHDFA scheme thanks to a systematic blue shift in the excitation energies. In addition, we see that the SCS or SOS variants of global methods reduce the RMSD by half, e.g, TD(A)-B2PLYP and TD(A)-B2GP-PLYP.

Inspecting the TDA-DHDFA results for LC-DHDFAs, SOS-RSX-QIDH is the best tested method with an RMSD of 0.20 eV, closely followed by SOS-ωB88PP86 and SOS-ωPBEPP86. Three more SCS/SOS LC-DHDFAs follow before the first global DHDFA appears in the ranking, namely, SCS-B2GP-PLYP21 with an RMSD of 0.26 eV, sharing the same value as SCS/SOS-ωB2PLYP. Next, we have SCS-ωPBEPP86, SOS-B2GP-PLYP21, PBE-QIDH's SCS and SOS variants, alongside SCS-RSX-QIDH with values ranging from 0.27 to 0.29 eV. Most of the remaining methods display RMSDs that range from 0.30 eV (PBE-QIDH, SCS-PBE-QIDH, and ωB88PP86) to 0.66 eV (B2PLYP).

For the TD-DHDFA results, it is noticeable

Table 7: Statistical results (in eV) for the full CT set using TDA (left) and full TD algorithms (right).[a]

	TDA-DHDFA					TD-DHDFA			
Method	MD	MAD	RMSD	Δ_{err}	Method	MD	MAD	RMSD	Δ_{err}
SOS-RSX-QIDH	0.05	0.17	0.20	0.70	SOS-ωB2GP-PLYP	0.03	0.12	0.15	0.47
SOS-ωB88PP86	0.05	0.15	0.21	0.80	SCS-ωB2GP-PLYP	0.00	0.12	0.16	0.57
SOS-ωPBEPP86	0.01	0.16	0.22	0.82	SCS/SOS-ωB2PLYP	0.07	0.12	0.16	0.48
SCS-ωB2GP-PLYP	0.11	0.17	0.23	0.75	SOS-ωB88PP86	–0.04	0.14	0.18	0.68
SOS-ωB2GP-PLYP	0.14	0.18	0.23	0.65	SCS-ωB88PP86	0.00	0.13	0.19	0.73
SCS-ωB88PP86	0.09	0.18	0.24	0.85	SOS-RSX-QIDH	–0.06	0.16	0.19	0.53
SCS-B2GP-PLYP21	–0.08	0.19	0.26	0.94	SOS-ωPBEPP86	–0.08	0.16	0.20	0.69
SCS/SOS-ωB2PLYP	0.18	0.21	0.26	0.66	ωB2PLYP	0.15	0.18	0.23	0.61
SCS-ωPBEPP86	–0.03	0.21	0.27	1.02	ωB2GP-PLYP	0.15	0.19	0.23	0.64
SOS-B2GP-PLYP21	–0.13	0.21	0.28	0.95	ωB88PP86	0.01	0.17	0.24	0.92
SOS-PBE-QIDH	–0.15	0.22	0.29	0.89	SCS-RSX-QIDH	–0.03	0.18	0.24	0.87
SCS-RSX-QIDH	0.07	0.22	0.29	1.06	SCS-B2GP-PLYP21	–0.15	0.20	0.25	0.78
SCS-PBE-QIDH	–0.15	0.23	0.30	0.95	ωPBEPP86	0.00	0.19	0.26	0.96
PBE-QIDH	–0.05	0.24	0.30	1.07	SCS-ωPBEPP86	–0.12	0.21	0.27	0.89
ωB88PP86	0.09	0.24	0.30	1.04	SOS-B2GP-PLYP21	–0.20	0.23	0.29	0.79
ωPBEPP86	0.08	0.25	0.31	1.09	PBE-QIDH	–0.08	0.23	0.29	0.92
SCS/SOS-B2PLYP21	–0.12	0.26	0.34	1.14	SOS-PBE-QIDH	–0.18	0.23	0.30	0.81
ωB2GP-PLYP	0.26	0.30	0.34	0.84	SCS-PBE-QIDH	–0.17	0.24	0.31	0.84
ωB2PLYP	0.27	0.29	0.35	0.80	RSX-QIDH	0.28	0.29	0.33	0.59
B2GP-PLYP	–0.28	0.34	0.44	1.17	SCS/SOS-B2PLYP21	–0.20	0.27	0.34	0.98
RSX-QIDH	0.40	0.41	0.45	0.80	B2GP-PLYP	–0.34	0.36	0.45	1.02
B2PLYP	–0.53	0.57	0.66	1.33	B2PLYP	–0.58	0.59	0.69	1.18

[a] The dipeptid, β-peptide, and PP calculations were performed with the cc-pVTZ AO basis set. The B-TCNE, DMABN, pNA, and HCl calculations were performed with the aug-cc-pVTZ AO basis set. The DBQ calculation was performed with the def2-TZVPP[134] AO basis set.

that ωB2GP-PLYP's SCS and SOS variants have significantly lowered their RMSDs compared to the TDA-DHDFA values, namely from 0.23 to 0.15/0.16 eV, which position them as the best TD-DHDFA methods. In total, there are seven new SCS/SOS-LC-DHDFA methods that all have RMSDs below 0.2 eV and surpass the previously reported best results for ωB2PLYP and ωB2GP-PLYP (RMSD = 0.23 eV). The remaining methods in this ranking are listed in Table 7; similar to the TDA-DHDFA scheme, TD-B2PLYP is the worst DHDFA with an RMSD of 0.69 eV.

In Ref. 83, the RS-DH methods were assessed on a slightly modified version of our CT set[40] and only for the TDA-DHDFA scheme. Therein, our peptides were excluded from the analysis. In order to compare our methods with those, we included an additional analysis that omits those systems in the SI. We briefly mention that there is a small decrease in the RMSDs for some methods, for instance, a reduction of 0.02 eV for SOS-RSX-QIDH, 0.03 eV for SOS-ωB88PP86. However, the general trend remains the same. The RS-DH methods are positioned after the SCS and SOS variants of our own LC-DHDFAs, with RMSDs slightly above 0.30 eV. Ref. 85 did not assess CT transitions for the scaled RS-DH methods with the same set as ours, which is why we cannot provide a comparison here.

6 Cross-Validation for Vertical Singlet-Triplet Excitations

After having presented promising results for vertical singlet-singlet excitations, we shift our attention to the discussion of vertical singlet-triplet excitations. The first study of such excitations was done in 2007 for the TDA-B2PLYP functional,[18] where Grimme and Neese examined 22 excitations in seven different systems based on experimental data. In 2020, we assessed the TDA-DHDFAs idea for the second time and, for the first time, TD-DHDFAs for such excitations in a more comprehensive study.[41] Our study showed that like other functionals TD-DHDFAs are not useful for such excitations, but that TDA-DHDFAs can provide accurate results. Herein, we follow up on our study from 2020. Note that there is no data available for such excitations for RS-B88-LYP and RS-PBE-PBE, and they will not be considered in the following.

6.1 The Loos and Jacquemin Benchmark Set

The original benchmark set by Loos, Jacquemin, and co-workers comprises 47 singlet-triplet transitions, of which we selected 35 transitions (23 local valence, 12 Rydberg,

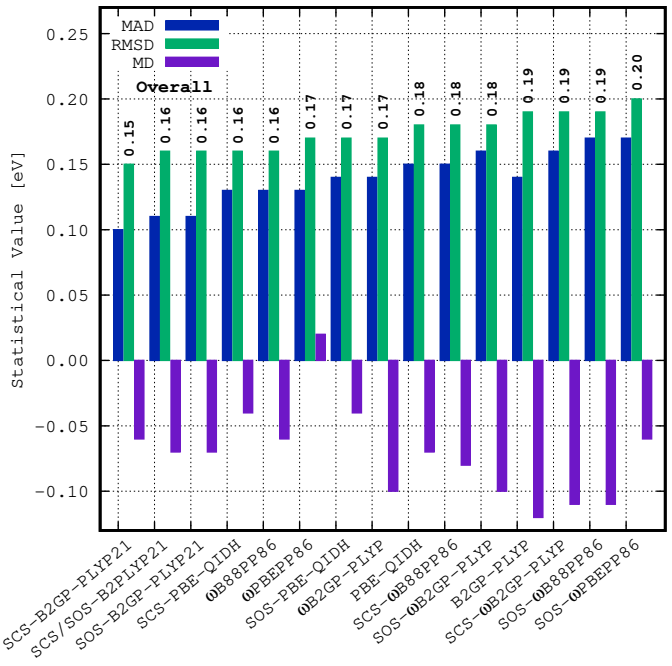

Figure 5: Statistical values (in eV) for the S0-TN transitions for the complete Loos and Jacquemin set, namely RMSDs (values shown over each bar), MADs, and MDs. Only the best 15 methods are shown; values for all assessed methods and a breakdown of the statistics into local-valence and Rydberg excitations can be found in the SI. The aug-cc-pVTZ AO basis set was used in all cases.

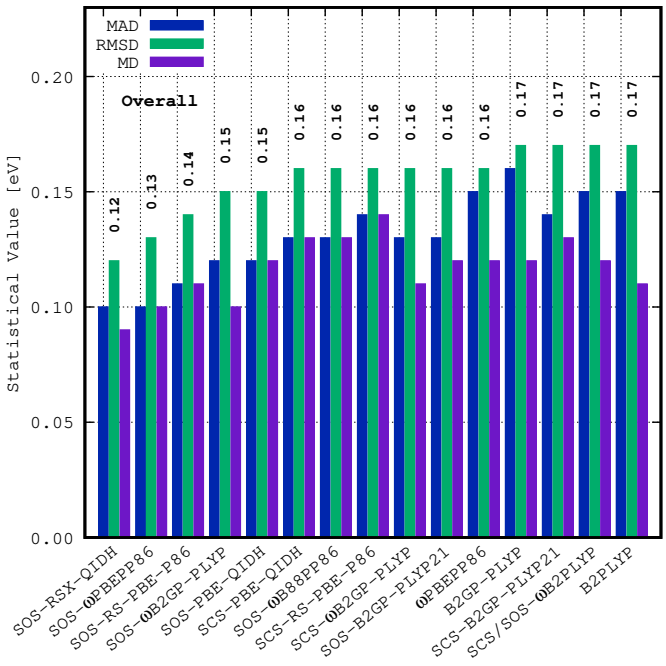

Figure 6: Statistical values (in eV) for the S1-T1 energy splitting on the Loos and Jacquemin set, namely RMSDs (values shown over each bar), MADs, and MDs. Only the best 15 methods are shown; values for all assessed methods can be found in the SI. The values for the SCS/SOS-RS-DH methods, excluding HCl, were taken from Ref. 85. The aug-cc-pVTZ AO basis set was used in all cases.

and one CT state) in 13 different molecules, which have not been included in other herein discussed sets. All references are of CC3/aug-cc-pVTZ quality and taken from Ref. 118, except for HCl, which was calculated by us and reported in Ref. 41. Note that Ref. 85 did not include HCl, but this difference is negligible for the statistics reported for our methods.

6.1.1 All Singlet-Triplet Excitations in this set (S0-TN)

Fig. 5 shows the same trend as in the updated Gordon set in Section 4.2.3, thus, confirming the reliability of our new methods. We note that (SCS/SOS)-RS-DH methods do not appear in the top 15 for this set. Similar to the updated Gordon set, our methods again perform very well, with SCS-B2GP-PLYP21 being the first method in our ranking (0.15 eV), closely followed by SCS/SOS-B2PLYP21, SOS-B2GP-PLYP21, ωB88PP86, and SCS-PBE-QIDH. Furthermore, ωPBEPP86, ωB2GP-PLYP, SOS-PBE-QIDH, SCS-ωB88PP86, the unscaled PBE-QIDH, and SOS-ωB2GP-PLYP perform very well with RMSDs of about 0.18 eV. The last three methods with RMSDs below 0.2 eV are B2GP-PLYP, SCS-ωB2GP-PLYP, and SOS-ωB88PP86. Other results are shown in the SI and we just point out that we obtained the largest RMSDs for RSX-QIDH, SOS-RS-PBE-P86 and B2PLYP with values beyond 0.23 eV. The MDs display the same trend as in the updated Gordon set by showing a systematic underestimation for the S0-TN transitions.

6.1.2 S1-T1 Analysis

Despite global DHDFAs leading the S0-TN analysis, LC-DHDFAs are the best for the S1-T1 energy splitting, as can be seen in Fig. 6, where SOS-RSX-QIDH and SOS-ωPBEPP86 display very good RMSDs of about 0.12 eV, slightly above the "chemical accuracy" threshold. Besides those two, there are other 17 methods that perform very well with RMSDs below 0.2 eV, eight of which are SCS/SOS-LC-DHDFAs (see Fig. 6). Surprisingly, there are two SCS/SOS methods that are positioned above 0.2 eV, namely, SCS/SOS-B2PLYP21

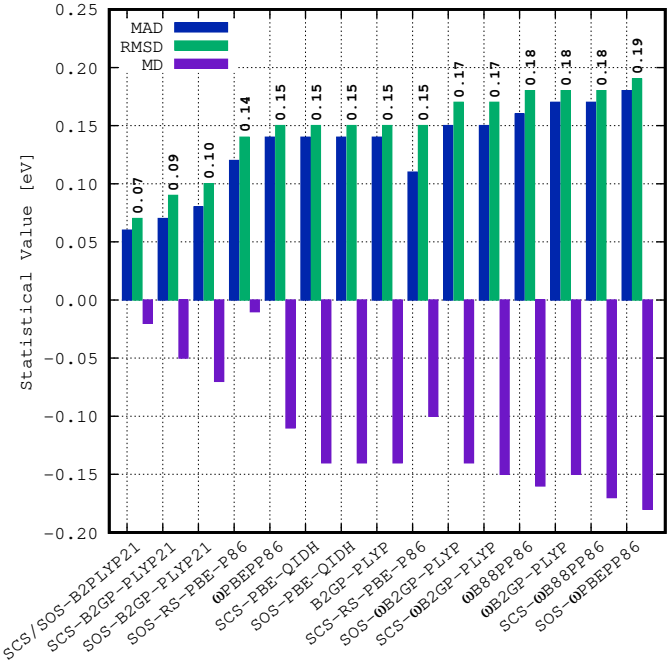

Figure 7: Statistical values (in eV) for the S0-TN transitions for the "Exotic-Molecules" set, namely RMSDs (values shown over each bar), MADs, and MDs. Only the best 15 methods are shown; values for all assessed methods can be found in the SI. The values for the SCS/SOS-RS-DH methods were taken from Ref. 85. The aug-cc-pVTZ AO basis set was used in all cases.

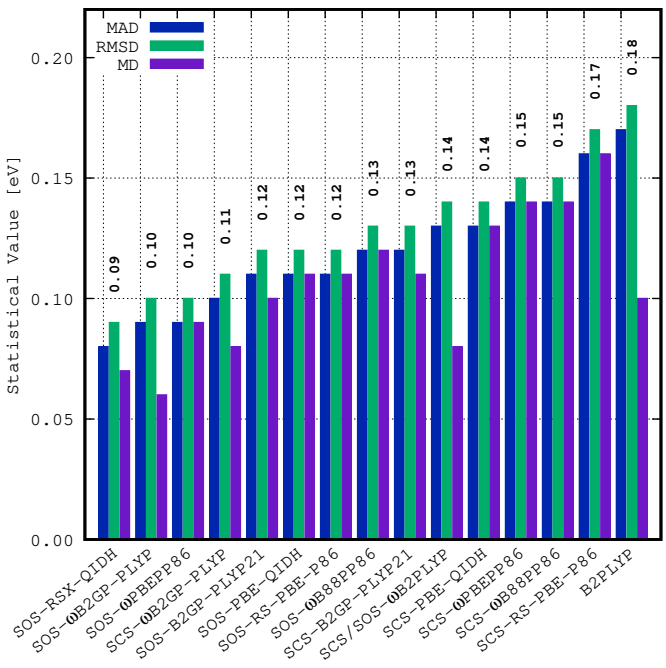

Figure 8: Statistical values (in eV) for the S1-T1 energy splitting on the "Exotic-Molecules" set, namely RMSDs (values shown over each bar), MADs, and MDs. Only the best 15 methods are shown; values for all assessed methods can be found in the SI. The values for the SCS/SOS-RS-DH methods were taken from Ref. 85. The aug-cc-pVTZ AO basis set was used in all cases.

which was the second-best in the S0-TN analysis, and SCS-RSX-QIDH. The worst performer is the unscaled RSX-QIDH with an RMSD of 0.27 eV.

The MDs follow the same trend as in the updated Gordon set, with a systematic underestimation in the excitation energies for the S0-TN analysis, whereas there is a systematic overestimation for the S1-T1 energy splitting. In the remaining sections, we will see that this is a general trend and cease to comment on MDs.

6.2 The "Exotic-Molecules" Set

This set by Loos, Jacquemin, and co-workers[119] consists of 11 singlet-triplet transitions of local-valence character in seven different systems, all of high-level CC3/aug-cc-pVTZ quality.

6.2.1 All Singlet-Triplet Excitations in this set (S0-TN)

Similar to Section 6.1.1, the SCS and SOS variants of B2PLYP and B2GP-PLYP are also the best methods here, with low RMSDs that range from 0.07 eV for SCS/SOS-B2PLYP21 to 0.10 eV for SOS-B2GP-PLYP21 (Fig. 7). Somewhat higher in energy, SOS-RS-PBE-P86 has an RMSD of 0.14 eV, ωPBEPP86, SCS- and SOS-PBE-QIDH, B2GP-PLYP, and SCS-RS-PBE-P86 share the same RMSD of 0.15 eV. ωB2GP-PLYP's SCS and SOS variants, ωB88PP86, SOS-ωB88PP86, and the unscaled ωB2GP-PLYP follow next in the ranking. The last DHDFA with an RMSD below 0.2 eV is SOS-ωPBEPP86 with an RMSD of 0.19 eV. The remaining scaled and unscaled methods display results that range from 0.20 eV (SCS/SOS-ωB2PLYP) to 0.25 eV (RSX-QIDH).

6.2.2 S1-T1 Analysis

The S1-T1 splitting shows the same behavior as in the previous set (Fig. 8). The SOS variants of RSX-QIDH, ωB2GP-PLYP, and ωPBEPP86 are the best three performers with RMSDs within the chemical accuracy threshold of 0.10 eV. Other methods that also display excellent results are SCS-ωB2GP-PLYP, B2GP-PLYP, PBE-QIDH, SOS-RS-PBE-P86, and SOS-ωB88PP86 with values near 0.12 eV. SCS/SOS-

ωB2PLYP, SCS-PBE-QIDH, SCS-ωPBEPP86, and SCS-ωB88PP86 perform similarly with RMSDs of up to 0.15 eV. SCS-RS-PBE-P86 has an RMSD of 0.17 eV, and B2PLYP is the first unscaled method in the list and shares the same RMSD of 0.18 eV with SCS/SOS-B2PLYP21, B2GP-PLYP, and ωPBEPP86. The remaining methods have RMSDs ranging from 0.20 eV (SCS-RSX-QIDH) to 0.29 eV (RSX-QIDH).

6.3 The Thiel Benchmark Set

The original set by Thiel and co-workers comprises 63 triplet excitations with CC3/TZVP[27] reference values. However, most of the molecules have already been addressed in our preceding analyses and therefore we decided to study only six molecules that have not been assessed before, namely, acetamide, benzoquinone, imidazole, naphthalene, norbornadiene, and octatetraene. For these six molecules, a total of 25 local-valence excitations need to be analyzed.

6.3.1 All Singlet-Triplet Excitations in this set (S0-TN)

The RMSDs are below 0.2 eV for almost every tested method (see Fig. 9). SCS/SOS-B2PLYP21 and the new unscaled DHDFAs, ωB88PP86 and ωPBEPP86, are positioned as the best three methods with RMSDs slightly above the chemical accuracy threshold. There are 16 methods with RMSDs below 0.2 eV, eight of which are SCS/SOS-LC-DHDFAs. Surprisingly, we find ωB2GP-PLYP's SCS and SOS variants among the worst-performing methods with an RMSD of 0.22 eV, followed by SOS-RS-PBE-P86, the unscaled ωB2GP-PLYP, RSX-QIDH, and B2PLYP (for more details, see SI).

6.3.2 S1-T1 Analysis

Note that Thiel and co-workers argued that the first singlet-singlet excited state in imidazole was of n – π* type and has 1^1A" symmetry.[27] However, after closer inspection of their CC3 reference data provided in the same work we found that the first singlet excited state should be of π – π* character and have 2^1A' symmetry.

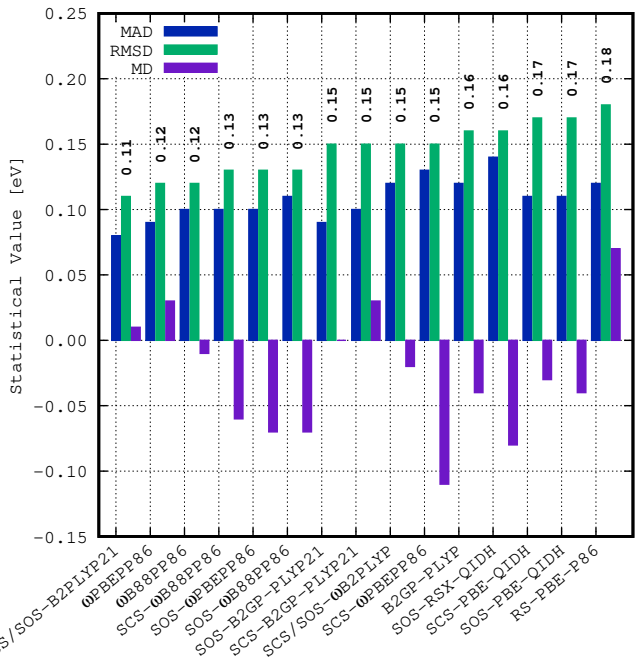

Figure 9: Statistical values (in eV) for the S0-TN transitions for the Thiel set, namely RMSDs (values shown over each bar), MADs, and MDs. Only the best 15 methods are shown; values for all assessed methods can be found in the SI. The values for the RS-DH method were taken from Ref. 83. The TZVP AO basis set was used in all cases.

In light of this finding, Fig. 10 includes both analyses with the values based on the π – π* transition given in parentheses.

The RMSDs for the S1-T1 splitting are higher than in previous sets when the π – π* type singlet excited state for imidazole is taken into account: now the RMSDs (values in parentheses in Fig. 10) range from 0.20 eV (SOS- and SCS-B2GP-PLYP21, SOS-PBE-QIDH, SOS-ωPBEPP86, and SOS-RS-PBE-P86) to 0.36 eV (RSX-QIDH). Nevertheless, most of the SCS or SOS variants still display similar behavior as in previous sets, with SCS-RSX-QIDH being the only exception with an RMSD of 0.30 eV. Similarly, the unscaled PBE-QIDH (0.28 eV), ωB2GP-PLYP (0.28 eV), ωB2PLYP (0.30 eV), and RSX-QIDH are positioned last.

If we now consider the n – π* type singlet excited state in imidazole, the RMSDs are greatly improved by about 0.08 eV. In this picture, the best six methods are all SOS variants with RMSDs of 0.12-0.13 eV. Next, we identify another seven methods all of which are SCS variants, alongside SOS-RS-PBE-P86, with RMSDs of up to 0.15 eV. ωPBEPP86 is

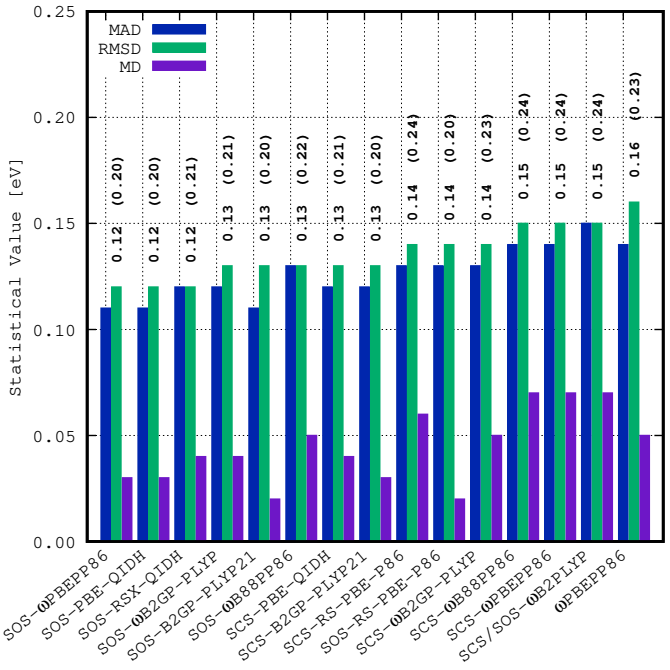

Figure 10: Statistical values (in eV) for the S1-T1 energy splitting on the Thiel set, namely RMSDs (values shown over each bar), MADs, and MDs The methods are sorted according to their overall RMSDs by considering the singlet excited state of $n-\pi^*$ type (1^1A'' symmetry) in imidazole. RMSDs based on the $\pi-\pi^*$ transition in imidazole (2^1A' symmetry) are shown in parentheses. Only the best 15 methods are shown; values for all assessed methods can be found in the SI. The values for the SCS/SOS-RS-DH methods were taken from Ref. 85. The TZVP AO basis set was used in all cases.

the first unscaled DHDFA and shares the same RMSD as SCS/SOS-B2PLYP21 of 0.16 eV. The unscaled DHDFAs ωB88PP86, B2GP-PLYP, PBE-QIDH, ωB2GP-PLYP, SCS-RSX-QIDH, and RS-PBE-P86 are the last six methods with RMSDs below 0.2 eV. Lastly, B2PLYP, ωB2PLYP, and RSX-QIDH are positioned last.

7 Overall Performance

In the spirit of the GMTKN55 database for ground state main-group thermochemistry, kinetics, and noncovalent interactions[8] we perform two additional analyses that help identify those methods that distinguish themselves from others according to their overall performance and robustness. In order to achieve such an analysis, we opted for two different strategies: (a) we order the TDA-DHDFAs by their RMSDs for each set and then rank them according to how many times a certain method yields the three best or three worst RMSDs and (b) we rank them by their averaged MAD or RMSD ($\overline{\text{MAD}}/\overline{\text{RMSD}}$) in the TDA-DHDFA framework according to

$$\overline{\text{MAD}}/\overline{\text{RMSD}} = \frac{\sum_{\text{i}}^{14} (\text{MAD}/\text{RMSD})_{\text{i}}}{14}, \quad (17)$$

where the sum runs over each of the 14 individual sets and $(\text{MAD}/\text{RMSD})_{\text{i}}$ is the MAD/RMSD of the respective method for the i^{th} set. Note that the CT set is excluded as no sufficient data for this set was available for all (SCS/SOS-)RS-DH methods. All other singlet excitation sets are included in the number 14, in addition to the separate S0-TN and S1-T1 analyses, which were considered as individual sets.

7.1 Top-Three Best/Worst Analysis

We begin with some general comments on how this analysis was performed. In almost every set we observed that multiple methods yielded the same RMSD. For instance, in the overall analysis of the ωB2(GP-)PLYP training set, there are three methods that share the best RMSD of 0.12 eV (SCS-RS-PBE-P86, and PBE-QIDH's SCS and SOS variants). Therefore, we assign the first position to each of them. We repeat the same strategy also for the second, third, and last three positions for every set. The outcome of our analysis is shown in Fig. 11.

SCS-PBE-QIDH is one of the most robust functionals in this work and is at the top ten times. However, we have to emphasize that this method does not outperform TDA-LC-DHDFAs for CT transitions, and the difference is even larger if we consider the TD-LC-DHDFA results (see Section 5.6 and SI). Our new SOS-ωPBEPP86 is another well-performing functional and is one of the top-three methods nine times. It also comes with the advantage of performing well regardless of the type of excitation, incl. CT ones. If the nature of the transition is unknown, SOS-ωPBEPP86 is therefore robust enough to give reliable results. SOS-ωB88PP86, SOS-PBE-QIDH, and SOS-B2GP-PLYP21 can also be recommended, keeping in

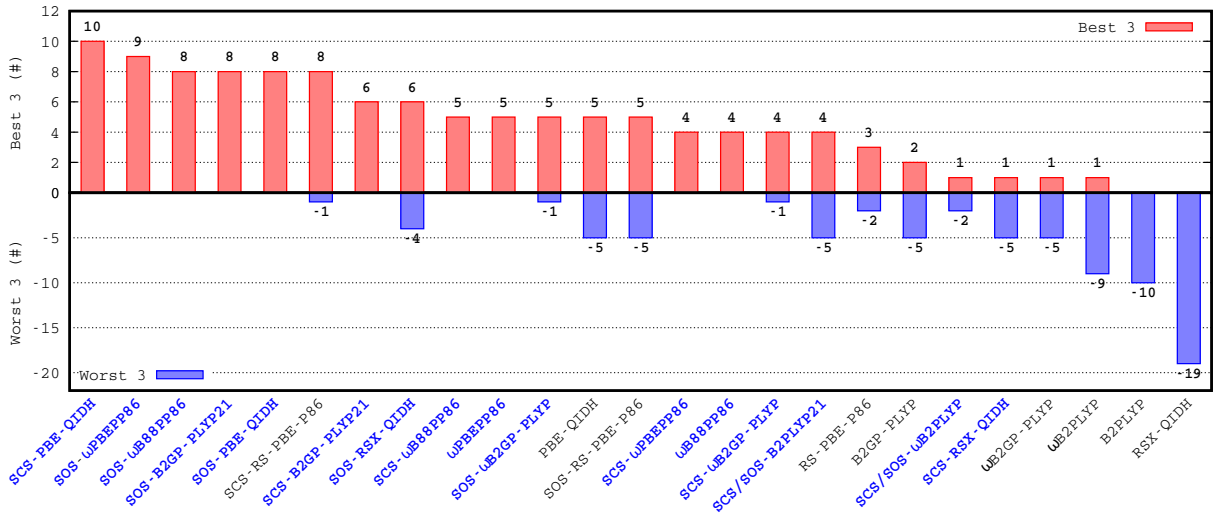

Figure 11: Analysis of how many times a method yields the three best and three worst RMSDs in a benchmark set. Methods highlighted in blue have been introduced in this work. The values for the (SCS/SOS-)RS-DH methods were taken from Refs 83 and 85. Our CT set was not included in this analysis given that the (SCS/SOS-)RS-DH methods had not been assessed on it.

mind that the first outperforms the latter two for CT transitions. SCS-RS-PBE-P86 is another well-performing method. Nevertheless, it shows to be less robust than its three predecessors by ranking among the worst three methods once. Indeed, SCS-B2GP-PLYP21 shows to be more robust despite being among the top methods only six times. SOS-RSX-QIDH is also somewhat less robust given that it ranks among the worst three methods four times. Some other methods that we recommend are SCS-ωB88PP86, ωPBEPP86, SCS-ωPBEPP86, and ωB88PP86 . Even though the first two only rank at the top three five and the latter two four times, they never appear among the worst-ranked functionals. The remaining methods display less robust behavior and can not be recommended for future applications to unexplored problems if a functional of general robustness is required.

7.2 Averaged MAD/RMSD Analysis

In Fig. 12, we present the $\overline{\text{MAD}}$ and $\overline{\text{RMSD}}$ values for the present work. Their trends seem to be similar to the previous analysis, where SCS and SOS-PBE-QIDH are on top of the list with the best results of just 0.14 eV for $\overline{\text{RMSD}}$, which are closely followed by five methods that display same value of 0.15 eV, of which three are SOS-LC-DHDFAs, namely, the SOS variants of ωPBEPP86, ωB88PP86, and ωB2GP-PLYP. Other methods that we also recommend are SCS- and SOS-B2GP-PLYP21, SCS-ωB2GP-PLYP, SCS-RS-PBE-P86, and SCS-ωB88PP86. Nevertheless, the scaled variants of PBE-QIDH and B2GP-PLYP21 should be used with care due to their inability to describe CT transitions. On the other hand, ωPBEPP86 is the best unscaled method which even rivals some SCS and SOS methods, i.e., SOS-RS-PBE-P86, SCS-ωPBEPP86, SCS/SOS-ωB2PLYP, and SOS-RSX-QIDH. The last four methods with results below 0.2 eV are the unscaled ωB88PP86, B2GP-PLYP, RS-PBE-P86, and the scaled SCS/SOS-B2PLYP21 . The remaining methods display values of or above 0.2 eV, with B2PLYP and RSX-QIDH being the ones with the poorest results of 0.24 and 0.29 eV, respectively. Even though SCS and SOS-PBE-QIDH are at the top of the list, our new SCS/SOS-LC-DHDFA methods have an increased $\overline{\text{RMSD}}$ of only 0.01 eV and they can provide more reliable results for systems that might have mixed valence-CT character (see Fig. 12). Indeed, our SCS/SOS-LC-DHDFAs are more accurate not only for CT transitions but also for the assessed PAHs.

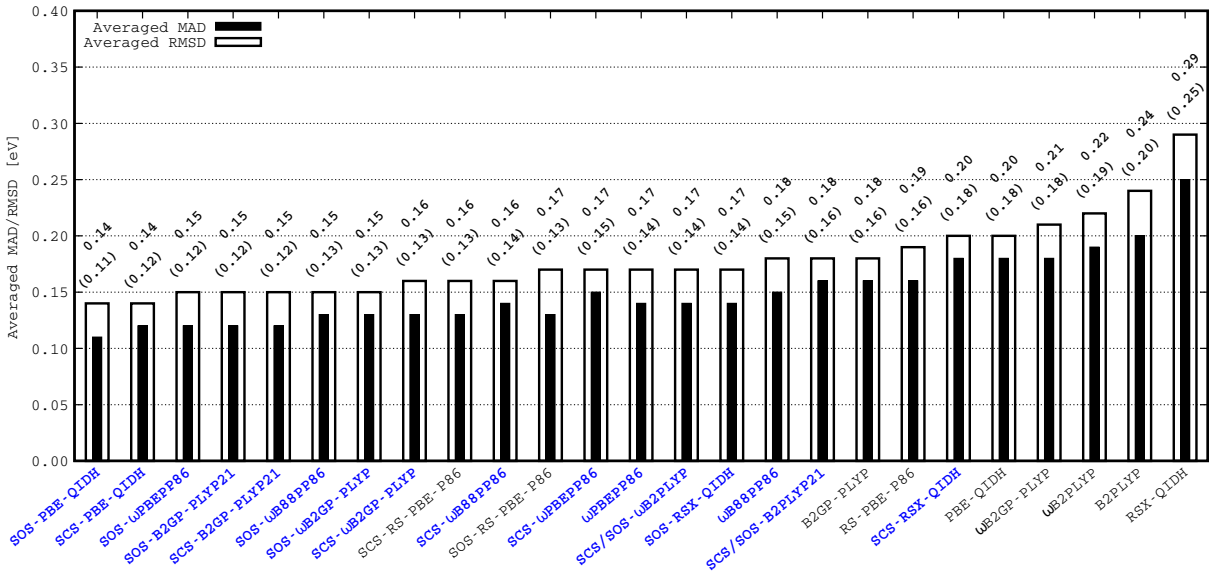

Figure 12: $\overline{\text{MAD}}/\overline{\text{RMSD}}$ analysis (in eV). The $\overline{\text{RMSD}}$s are shown as outlines and the $\overline{\text{MAD}}$s as solid bars. We also present their values above each bar, with the $\overline{\text{MAD}}$ in parentheses. The methods are sorted according to their $\overline{\text{RMSD}}$. Methods highlighted in blue have been introduced in this work. The values for the (SCS/SOS-)RS-DH methods were taken from Refs 83 and 85. Our CT set was not included in this analysis given that the (SCS/SOS-)RS-DH methods had not been assessed on it.

8 Conclusions

This has been the second time that SCS and SOS variants have been introduced and assessed for double hybrid density functional approximations (DHDFAs) for the computation of electronic excitation energies that follow the initial definition by Grimme and Neese (see Eq.7), in which the perturbative component is not range-separated. The main differences to the first work of this kind in 2017[39] are the incorporation of the latest LC-DHDFAs[40,83,101] and the analysis of singlet-triplet excitations. Note that the SCS/SOS variants here are based on the SCS/SOS-CIS(D) wavefunction methods according to which the so-called direct and indirect terms have to be scaled separately. Thus, our methods differ from the SCS/SOS-RS-PBE-P86 functionals that were published[85] while our present work was under review. We remind the reader that herein we already took into account the best TD(A)-DFT methods and improving them further poses a major challenge. We compared unscaled DHDFAs with new SCS and SOS variants and tested those on six benchmark sets that comprised 203 unique excitations in small to medium-sized molecules and different excitation types. While most of this work focused mostly on the Tamm-Dancoff approximation (TDA-DHDFAs), we also presented results based on full TD-DHDFAs for the PAH and CT benchmark sets.

We confirmed the good accuracy and robustness of DHDFAs for the computation of electronic excitation energies. In general, they showed the same accuracy as previous studies. The introduction of SCS and SOS caused a systematic red-shift in the excitation energies, contrary to the previous observations made by Schwabe and Goerigk in 2017.[39] Sometimes, the red-shift eliminated extreme outliers in the excitation energies, thus reducing error spans by up to 0.3 eV. The only exceptions to this are the BLYP-based global DHDFAs B2PLYP and B2GP-PLYP, which displayed a blue-shift in the excitation energies. One benefit of using SCS and SOS is a more balanced description compared to the reference values, with MDs usually being closer to zero. Our SCS and SOS variants also showed that it is not necessary to include a long-range correction in the perturbative part of a DHDFA to obtain reasonable results. In fact, the five methods following that approach were outperformed by many of our newly presented ones.

One important finding is that we did not see any particular trend of when to prefer SCS over SOS or vice-versa for our approaches. In

fact, SCS and SOS variants present negligible differences in the RMSDs of up to 0.03 eV when applied to DHDFAs. Note that this is contrary to some ground state wave function methods where SOS can lead to inferior results compared to SCS, compromising accuracy and efficiency.[7,10] Accurate SOS-DHDFAs provide faster calculation of larger systems and might also open a route to more efficient methods for the optimization of excited-state geometries once the Laplace transform is applied, similar to its wave function counterpart.

While unscaled TD(A)-DHDFAs already constitute an improvement over conventional TD(A)-DFT methods, as conclusively shown in the literature,[18,28,33–36,40,41] we recommend specific new SCS- and SOS-based variants presented in this work for further testing and subsequent applications. Based on our averaged MAD/RMSD analysis, we highly recommend our SCS and SOS variants of PBE-QIDH, ωB88PP86, and ωPBEPP86. That being said, SCS- and SOS-PBE-QIDH are not suitable for the computation of CT excitations, and the SCS/SOS-ωB88PP86 and SCS/SOS-ωPBEPP86 should be employed instead. Indeed, the latter four methods can provide accurate excitation energies regardless of the type of transition, making them more robust for real applications to new systems. Finally, if only unscaled DHDFAs are available to the user, we strongly recommend ωPBEPP86 as the best-unscaled method, which outperformed some other SCS and SOS methods presented in this work.

Our work showed once more that TD(A)-DHDFAs have their place in the treatment of accurate electronic excitation energies. All our newly presented methods are available in the very recently released ORCA5. Finally, we would like to encourage the implementation of TD(A)-DHDFAs with and without SCS/SOS into other standard software packages.

Acknowledgement M.C.-P. acknowledges a 'Melbourne Research Scholarship' by The University of Melbourne. L. G. acknowledges generous allocation of resources by the National Computational Infrastructure (NCI) National Facility within the National Computational Merit Allocation Scheme (project ID: fk5) and Research Platform Services (ResPlat) at The University of Melbourne (Project No. punim0094). This research was also supported by the sustaining and strengthening merit-based access to the NCI LIEF Grant (LE190100021) facilitated by The University of Melbourne.

Supporting Information Available

The Supplementary Information includes all references values, excitation energies and statistical values for all tested cases and density functional approximations in two seperate xlsx files. Those files are available free of charge.

References

(1) Hohenberg, P.; Kohn, W. Inhomogeneous electron gas. *Phys. Rev. B* **1964**, *136*, 864–871.

(2) Kohn, W.; Sham, L. J. Self-consistent equations including exchange and correlation effects. *Phys. Rev.* **1965**, *140*, A1133–A1138.

(3) Runge, E.; Gross, E. K. U. Density-functional theory for time-dependent systems. *Phys. Rev. Lett.* **1984**, *52*, 997–1000.

(4) Bauernschmitt, R.; Ahlrichs, R. Treatment of electronic excitations within the adiabatic approximation of time dependent density functional theory. *Chem. Phys. Lett* **1996**, *256*, 454–464.

(5) Grimme, S. Semiempirical hybrid density functional with perturbative second-order correlation. *J. Chem. Phys.* **2006**, *124*, 034108.

(6) Goerigk, L.; Grimme, S. Efficient and accurate double-hybrid-meta-GGA density functionals-evaluation with the ex-

tended GMTKN30 database for general main group thermochemistry, kinetics, and noncovalent interactions. *J. Chem. Theory Comput.* **2011**, *7*, 291–309.

(7) Goerigk, L.; Grimme, S. A thorough benchmark of density functional methods for general main group thermochemistry, kinetics, and noncovalent interactions. *Phys. Chem. Chem. Phys.* **2011**, *13*, 6670–6688.

(8) Goerigk, L.; Hansen, A.; Bauer, C.; Ehrlich, S.; Najibi, A.; Grimme, S. A look at the density functional theory zoo with the advanced GMTKN55 database for general main group thermochemistry, kinetics and noncovalent interactions. *Phys. Chem. Chem. Phys.* **2017**, *19*, 32184–32215.

(9) Mardirossian, N.; Head-Gordon, M. Survival of the most transferable at the top of jacob's ladder: defining and testing the ωB97M(2) double hybrid density functional. *J. Chem. Phys.* **2018**, *148*, 241736.

(10) Mehta, N.; Casanova-Páez, M.; Goerigk, L. Semi-empirical or non-empirical double-hybrid density functionals: which are more robust? *Phys. Chem. Chem. Phys.* **2018**, *20*, 23175–23194.

(11) Kozuch, S.; Gruzman, D.; Martin, J. M. L. DSD-BLYP: A general purpose double hybrid density functional including spin component scaling and dispersion correction. *J. Phys. Chem. C* **2010**, *114*, 20801–20808.

(12) Kozuch, S.; Martin, J. M. L. DSD-PBEP86: in search of the best double-hybrid DFT with spin-component scaled MP2 and dispersion corrections. *Phys. Chem. Chem. Phys.* **2011**, *13*, 20104–20107.

(13) Kozuch, S.; Martin, J. M. L. Spin-component-scaled double hybrids: an extensive search for the best fifth-rung functionals blending DFT and perturbation theory. *J. Comput. Chem.* **2013**, *34*, 2327–2344.

(14) Santra, G.; Sylvetsky, N.; Martin, J. M. L. Minimally empirical double-hybrid functionals trained against the GMTKN55 database: revDSD-PBEP86-d4, revDOD-PBE-d4, and DOD-SCAN-d4. *J. Phys. Chem. C* **2019**, *123*, 5129–5143.

(15) Martin, J. M. L.; Santra, G. Empirical double-hybrid density functional theory: A 'third way' in between WFT and DFT. *Isr. J. Chem.* **2019**, *60*, 787–804.

(16) Santra, G.; Cho, M.; Martin, J. M. L. Exploring avenues beyond revised DSD functionals: I. range separation, with xDSD as a special case. *J. Phys. Chem. A* **2021**, *125*, 4614–4627.

(17) Santra, G.; Semidalas, E.; Martin, J. M. L. Exploring avenues beyond revised DSD functionals: II. random-phase approximation and scaled MP3 corrections. *J. Phys. Chem. A* **2021**, *125*, 4628–4638.

(18) Grimme, S.; Neese, F. Double-hybrid density functional theory for excited electronic states of molecules. *J. Chem. Phys.* **2007**, *127*, 154116.

(19) Head-Gordon, M.; Rico, R. J.; Oumi, M.; Lee, T. J. A doubles correction to electronic excited states from configuration interaction in the space of single substitutions. *Chemical Physics Letters* **1994**, *219*, 21–29.

(20) Hirata, S.; Head-Gordon, M. Time-dependent density functional theory within the Tamm-Dancoff approximation. *Chem. Phys. Lett.* **1999**, *314*, 291–299.

(21) Benighaus, T.; DiStasio, R. A.; Lochan, R. C.; Chai, J.-D.; Head-Gordon, M. Semiempirical double-hybrid

density functional with improved description of long-range correlation. *J. Phys. Chem. A* **2008**, *112*, 2702–2712.

(22) Zhang, I. Y.; Xu, X. Reaching a uniform accuracy for complex molecular systems: long-range-corrected XYG3 doubly hybrid density functional. *J. Phys. Chem. Lett.* **2013**, *4*, 1669–1675.

(23) Cornaton, Y.; Fromager, E. Double hybrid density-functional theory using the coulomb-attenuating method. *Int. J. Quantum Chem.* **2014**, *114*, 1199–1211.

(24) Hedegård, E. D.; Heiden, F.; Knecht, S.; Fromager, E.; Jensen, H. J. A. Assessment of charge-transfer excitations with time-dependent, range-separated density functional theory based on long-range MP2 and multiconfigurational self-consistent field wave functions. *J. Chem. Phys.* **2013**, *139*, 184308.

(25) Kalai, C.; Toulouse, J. A general range-separated double-hybrid density-functional theory. *J. Chem. Phys.* **2018**, *148*, 164105.

(26) Karton, A.; Tarnopolsky, A.; Lamère, J.-F.; Schatz, G. C.; Martin, J. M. L. Highly accurate first-principles benchmark data sets for the parametrization and validation of density functional and other approximate methods. derivation of a robust, generally applicable, double-hybrid functional for thermochemistry and thermochemical kinetics. *J. Phys. Chem. A* **2008**, *112*, 12868–12886.

(27) Schreiber, M.; Silva-Junior, M. R.; Sauer, S. P. A.; Thiel, W. Benchmarks for electronically excited states: CASPT2, CC2, CCSD, and CC3. *J. Chem. Phys.* **2008**, *128*, 134110.

(28) Goerigk, L.; Moellmann, J.; Grimme, S. Computation of accurate excitation energies for large organic molecules with double-hybrid density functionals. *Phys. Chem. Chem. Phys.* **2009**, *11*, 4611–4620.

(29) Brémond, É.; Adamo, C. Seeking for parameter-free double-hybrid functionals: the PBE0-DH model. *J. Chem. Phys.* **2011**, *135*, 024106.

(30) Chai, J.-D.; Mao, S.-P. Seeking for reliable double-hybrid density functionals without fitting parameters: the PBE0-2 functional. *Chem. Phys. Lett.* **2012**, *538*, 121–125.

(31) Goerigk, L.; Grimme, S. Double-hybrid density functionals. *Wiley Interdiscip. Rev.: Comput. Mol. Sci.* **2014**, *4*, 576–600.

(32) Najibi, A.; Casanova-Páez, M.; Goerigk, L. Analysis of recent BLYP- and PBE-based range-separated double-hybrid density functional approximations for main-group thermochemistry, kinetics, and noncovalent interactions. *J. Phys. Chem. A* **2021**, *125*, 4026–4035.

(33) Goerigk, L.; Grimme, S. Calculation of electronic circular dichroism spectra with time-dependent double-hybrid density functional theory. *J. Phys. Chem. A* **2009**, *113*, 767–776.

(34) Goerigk, L.; Grimme, S. Assessment of TD-DFT methods and of various spin scaled CIS(D) and CC2 versions for the treatment of low-lying valence excitations of large organic dyes. *J. Chem. Phys.* **2010**, *132*, 184103.

(35) Goerigk, L.; Grimme, S. Double-hybrid density functionals provide a balanced description of excited ^1L_a and ^1L_b states in polycyclic aromatic hydrocarbons. *J. Chem. Theory Comput.* **2011**, *7*, 3272–3277.

(36) Goerigk, L.; Kruse, H.; Grimme, S. *Comprehensive chiroptical spectroscopy*; Wiley-Blackwell, 2012; pp 643–673.

(37) Meo, F. D.; Trouillas, P.; Adamo, C.; Sancho-García, J. C. Application of recent double-hybrid density functionals

to low-lying singlet-singlet excitation energies of large organic compounds. *J. Chem. Phys.* **2013**, *139*, 164104.

(38) Momeni, M. R.; Brown, A. A local CC2 and TDA-DFT double hybrid study on BODIPY/aza-BODIPY dimers as heavy atom free triplet photosensitizers for photodynamic therapy applications. *J. Phys. Chem. A* **2016**, *120*, 2550–2560.

(39) Schwabe, T.; Goerigk, L. Time-dependent double-hybrid density functionals with spin-component and spin-opposite scaling. *J. Chem. Theory Comput.* **2017**, *13*, 4307–4323.

(40) Casanova-Páez, M.; Dardis, M. B.; Goerigk, L. ωB2PLYP and ωB2GPPLYP: the first two double-hybrid density functionals with long-range correction optimized for excitation energies. *J. Chem. Theory Comput.* **2019**, *15*, 4735–4744.

(41) Casanova-Páez, M.; Goerigk, L. Assessing the Tamm–Dancoff approximation, singlet–singlet, and singlet–triplet excitations with the latest long-range corrected double-hybrid density functionals. *J. Chem. Phys.* **2020**, *153*, 064106.

(42) Goerigk, L.; Casanova-Páez, M. The trip to the density functional theory zoo continues: making a case for time-dependent double hybrids for excited-state problems. *Aust. J. Chem.* **2021**, *74*, 3–15.

(43) Casanova-Páez, M.; Goerigk, L. Global double hybrids do not work for charge transfer: A comment on "double hybrids and time-dependent density functional theory: an implementation and benchmark on charge transfer excited states". *J. Comput. Chem.* **2021**, *42*, 528–533.

(44) Christiansen, O.; Koch, H.; Jørgensen, P. The second-order approximate coupled cluster singles and doubles model CC2. *Chem. Phys. Lett.* **1995**, *243*, 409–418.

(45) Hellweg, A.; Grün, S. A.; Hättig, C. Benchmarking the performance of spin-component scaled CC2 in ground and electronically excited states. *Phys. Chem. Chem. Phys.* **2008**, *10*, 4119.

(46) Goerigk, L.; Grimme, S. Quantum chemical investigation of exciton coupling: super-molecular calculations of a merocyanine dimer aggregate. *ChemPhysChem* **2008**, *9*, 2467–2470.

(47) Grimme, S. Improved second-order møller-plesset perturbation theory by separate scaling of parallel- and antiparallel-spin pair correlation energies. *J. Chem. Phys.* **2003**, *118*, 9095–9102.

(48) Jung, Y.; Lochan, R. C.; Dutoi, A. D.; Head-Gordon, M. Scaled opposite-spin second order Møller–Plesset correlation energy: an economical electronic structure method. *J. Chem. Phys.* **2004**, *121*, 9793–9802.

(49) Grimme, S.; Goerigk, L.; Fink, R. F. Spin-component-scaled electron correlation methods. *Wiley Interdiscip. Rev.: Comput. Mol. Sci.* **2012**, *2*, 886–906.

(50) Chai, J.-D.; Head-Gordon, M. Long-range corrected double-hybrid density functionals. *J. Chem. Phys.* **2009**, *131*, 174105.

(51) Brémond, E.; Savarese, M.; Sancho-García, J. C.; Pérez-Jiménez, A. J.; Adamo, C. Quadratic integrand double-hybrid made spin-component-scaled. *J. Chem. Phys.* **2016**, *144*, 124104.

(52) Almlöf, J. Elimination of energy denominators in møller-plesset perturbation theory by a laplace transform approach. *Chem. Phys. Lett.* **1991**, *181*, 319–320.

(53) Rhee, Y. M.; Head-Gordon, M. Scaled second-order perturbation corrections to configuration interaction singles: efficient and reliable excitation energy methods. *J. Phys. Chem. A* **2007**, *111*, 5314–5326.

(54) Tozer, D. J.; Amos, R. D.; Handy, N. C.; Roos, B. O.; Serrano-Andrés, L. Does density functional theory contribute to the understanding of excited states of unsaturated organic compounds? *Mol. Phys.* **1999**, *97*, 859–868.

(55) Tozer, D. J. Relationship between long-range charge-transfer excitation energy error and integer discontinuity in Kohn–Sham theory. *J. Chem. Phys.* **2003**, *119*, 12697–12699.

(56) Dreuw, A.; Head-Gordon, M. Failure of time-dependent density functional theory for long-range charge-transfer excited states:the zincbacteriochlorin-bacteriochlorin and bacteriochlorophyll-spheroidene complexes. *J. Am. Chem. Soc.* **2004**, *126*, 4007–4016.

(57) Becke, A. D. Density-functional exchange-energy approximation with correct asymptotic behavior. *Phys. Rev. A* **1988**, *38*, 3098–3100.

(58) Lee, C.; Yang, W.; Parr, R. G. Development of the colle-salvetti correlation-energy formula into a functional of the electron density. *Phys. Rev. B* **1988**, *37*, 785–789.

(59) Pishchalnikov, R. Y.; Yaroshevich, I. A.; Slastnikova, T. A.; Ashikhmin, A. A.; Stepanov, A. V.; Slutskaya, E. A.; Friedrich, T.; Sluchanko, N. N.; Maksimov, E. G. Structural peculiarities of keto-carotenoids in water-soluble proteins revealed by simulation of linear absorption. *Phys. Chem. Chem. Phys.* **2019**, *21*, 25707–25719.

(60) Pollice, R.; Friederich, P.; Lavigne, C.; dos Passos Gomes, G.; Aspuru-Guzik, A. Organic molecules with inverted gaps between first excited singlet and triplet states and appreciable fluorescence rates. *Matter* **2021**, *4*, 1654–1682.

(61) Suleiman, O.; Panthi, D.; Adeyiga, O.; Odoh, S. O. Methane C-H activation by $[Cu_2O]^{2+}$ and $[Cu_3O_3]^{2+}$ in copper-exchanged zeolites: computational analysis of redox chemistry and X-ray absorption spectroscopy. *Inorg. Chem.* **2021**, *60*, 6218–6227.

(62) Gao, Z.; Chen, S.; Bai, Y.; Wang, M.; Liu, X.; Yang, W.; Li, W.; Ding, X.; Yao, J. A new perspective for evaluating the photoelectric performance of organic–inorganic hybrid perovskites based on the DFT calculations of excited states. *Phys. Chem. Chem. Phys.* **2021**, *23*, 11548–11556.

(63) Yaroshevich, I. A.; Maksimov, E. G.; Sluchanko, N. N.; Zlenko, D. V.; Stepanov, A. V.; Slutskaya, E. A.; Slonimskiy, Y. B.; Botnarevskii, V. S.; Remeeva, A.; Gushchin, I.; Kovalev, K.; Gordeliy, V. I.; Shelaev, I. V.; Gostev, F. E.; Khakhulin, D.; Poddubnyy, V. V.; Gostev, T. S.; Cherepanov, D. A.; Polívka, T.; Kloz, M.; Friedrich, T.; Paschenko, V. Z.; Nadtochenko, V. A.; Rubin, A. B.; Kirpichnikov, M. P. Role of hydrogen bond alternation and charge transfer states in photoactivation of the Orange Carotenoid Protein. *Commun. Biol.* **2021**, *4*, 539.

(64) Puget, M.; Shcherbakov, V.; Denisov, S.; Moreau, P.; Dognon, J.-P.; Mostafavi, M.; Le Caër, S. Reaction mechanisms of the degradation of fluoroethylene carbonate, an additive of lithium-ion batteries, unraveled by radiation chemistry. *Chem. Eur. J.* **2021**, *27*, 8185–8194.

(65) Curtis, K.; Panthi, D.; Odoh, S. O. Time-dependent density functional theory study of copper(II) oxo active sites for methane-to-methanol conversion in zeolites. *Inorg. Chem.* **2021**, *60*, 1149–1159.

(66) Adeyiga, O.; Suleiman, O.; Odoh, S. O. Copper-oxo active sites for methane C–H

activation in zeolites: molecular understanding of impact of methane hydroxylation on UV–Vis spectra. *Inorg. Chem.* **2021**, *60*, 8489–8499.

(67) Perdew, J. P.; Burke, K.; Ernzerhof, M. Generalized gradient approximation made simple. *Phys. Rev. Lett.* **1996**, *77*, 3865–3868.

(68) Brémond, É.; Sancho-García, J. C.; Pérez-Jiménez, Á. J.; Adamo, C. Communication: double-hybrid functionals from adiabatic-connection: the QIDH model. *J. Chem. Phys.* **2014**, *141*, 031101.

(69) Vintonyak, V. V.; Warburg, K.; Kruse, H.; Grimme, S.; Hübel, K.; Rauh, D.; Waldmann, H. Identification of thiazolidinones spiro-fused to indolin-2-ones as potent and selective inhibitors of the mycobacterium tuberculosis protein tyrosine phosphatase B. *Angew. Chem. Int. Ed.* **2010**, *49*, 5902–5905.

(70) Send, R.; Valsson, O.; Filippi, C. Electronic excitations of simple cyanine dyes: reconciling density functional and wave function methods. *J. Chem. Theory Comput.* **2011**, *7*, 444–455.

(71) Markworth, P. B.; Adamson, B. D.; Coughlan, N. J. A.; Goerigk, L.; Bieske, E. J. Photoisomerization action spectroscopy: flicking the protonated merocyanine-spiropyran switch in the gas phase. *Phys. Chem. Chem. Phys.* **2015**, *17*, 25676–25688.

(72) Prlj, A.; Sandoval-Salinas, M. E.; Casanova, D.; Jacquemin, D.; Corminboeuf, C. Low-lying $\pi\pi^*$ states of heteroaromatic molecules: A challenge for excited state methods. *J. Chem. Theory Comput.* **2016**, *12*, 2652–2660.

(73) Alipour, M. On the performance of time-dependent double-hybrid density functionals for description of absorption and emission spectra of heteroaromatic compounds. *Theor Chem Acc* **2016**, *135*, 1–8.

(74) Sancho-García, J. C.; Adamo, C.; Pérez-Jiménez, A. J. Describing excited states of [n]cycloparaphenylenes by hybrid and double-hybrid density functionals: from isolated to weakly interacting molecules. *Theo. Chem. Acc.* **2016**, *135*, 25.

(75) Brémond, É.; Savarese, M.; Pérez-Jiménez, Á. J.; Sancho-García, J. C.; Adamo, C. Speed-up of the excited-state benchmarking: double-hybrid density functionals as test cases. *J. Chem. Theory Comput.* **2017**, *13*, 5539–5551.

(76) Ottochian, A.; Morgillo, C.; Ciofini, I.; Frisch, M. J.; Scalmani, G.; Adamo, C. Double hybrids and time-dependent density functional theory: an implementation and benchmark on charge transfer excited states. *J. Comput. Chem.* **2020**, *41*, 1242–1251.

(77) Hernández-Martínez, L.; Brémond, E.; Pérez-Jiménez, A. J.; San-Fabián, E.; Adamo, C.; Sancho-García, J. C. Nonempirical (double-hybrid) density functionals applied to atomic excitation energies: A systematic basis set investigation. *Int. J. Quantum Chem.* **2020**, *120*, e26193.

(78) Brémond, É.; Ottochian, A.; Pérez-Jiménez, Á. J.; Ciofini, I.; Scalmani, G.; Frisch, M. J.; Sancho-García, J. C.; Adamo, C. Assessing challenging intra- and inter-molecular charge-transfer excitations energies with double-hybrid density functionals. *J. Comput. Chem.* **2021**, *42*, 970–981.

(79) Sears, J. S.; Koerzdoerfer, T.; Zhang, C.-R.; Brédas, J.-L. Communication: orbital instabilities and triplet states from time-dependent density functional theory and long-range corrected functionals. *J. Chem. Phys.* **2011**, *135*, 151103.

(80) Peach, M. J. G.; Tozer, D. J. Overcoming low orbital overlap and triplet instability

problems in TDDFT. *J. Phys. Chem. A* **2012**, *116*, 9783–9789.

(81) Peach, M. J.; Warner, N.; David J. Tozer, On the triplet instability in TDDFT. *Mol. Phys.* **2013**, *111*, 1271–1274.

(82) Rangel, T.; Hamed, S. M.; Bruneval, F.; Neaton, J. B. An assessment of low-lying excitation energies and triplet instabilities of organic molecules with an ab initio bethe-salpeter equation approach and the Tamm-Dancoff approximation. *J. Chem. Phys.* **2017**, *146*, 194108.

(83) Mester, D.; Kállay, M. A simple range-separated double-hybrid density functional theory for excited states. *J. Chem. Theory Comput.* **2021**, *17*, 927–942.

(84) see https://doi.org/10.26434/chemrxiv.14706042.v1 (accessed on 2 July 2021).

(85) Mester, D.; Kállay, M. Spin-scaled range-separated double-hybrid density functional theory for excited states. *J. Chem. Theory Comput.* **2021**, published online, DOI: 10.1021/acs.jctc.1c00422 (accessed on 6 July 2021).

(86) Marques, M.; Gross, E. Time-dependent density functional theory. *Annu. Rev. Phys. Chem.* **2004**, *55*, 427–455.

(87) Marques, M. A. L.; Ullrich, C. A.; Nogueira, F.; Rubio, A.; Burke, K.; Gross, E. K. U. *Time-dependent density functional theory*; Lecture notes in physics; Springer-Verlag, 2006.

(88) Mark E. Casida, In *Recent advances in density functional methods*; Chong, D. P., Ed.; World Scientific Singapore, 1995; pp 155–192.

(89) Gross, E. K. U.; Kohn, W. Time-dependent density-functional theory. *Advan. Quantum Chem.* **1990**, *21*, 255–291.

(90) McLachlan, A. D.; Ball, M. A. Time-dependent Hartree—Fock theory for molecules. *Rev. Mod. Phys.* **1964**, *36*, 844–855.

(91) Iikura, H.; Tsuneda, T.; Yanai, T.; Hirao, K. A long-range correction scheme for generalized-gradient-approximation exchange functionals. *J. Chem. Phys.* **2001**, *115*, 3540–3544.

(92) Møller, C.; Plesset, M. S. Note on an approximation treatment for many-electron systems. *Phys. Rev.* **1934**, *46*, 618–622.

(93) Sharkas, K.; Toulouse, J.; Savin, A. Double-hybrid density-functional theory made rigorous. *J. Chem. Phys.* **2011**, *134*, 064113.

(94) Grimme, S.; Izgorodina, E. I. Calculation of 0–0 excitation energies of organic molecules by CIS(D) quantum chemical methods. *Chem. Phys.* **2004**, *305*, 223–230.

(95) Neese, F. The ORCA program system. *Wiley Interdiscip. Rev.: Comput. Mol. Sci.* **2012**, *2*, 73–78.

(96) Neese, F. Software update: the ORCA program system, version 4.0. *Wiley Interdiscip. Rev.: Comput. Mol. Sci.* **2018**, *8*, e1327.

(97) Valeev, E. F. Libint: A library for the evaluation of molecular integrals of many-body operators over gaussian functions. **2020**,

(98) Vahtras, O.; Almlöf, J.; Feyereisen, M. Integral approximations for LCAO-SCF calculations. *Chem. Phys. Lett.* **1993**, *213*, 514 – 518.

(99) Weigend, F.; Köhn, A.; Hättig, C. Efficient use of the correlation consistent basis sets in resolution of the identity MP2 calculations. *J. Chem. Phys* **2002**, *116*, 3175–3183.

(100) Chai, J.-D.; Head-Gordon, M. Systematic optimization of long-range corrected hybrid density functionals. *J. Chem. Phys.* **2008**, *128*, 084106.

(101) Brémond, É.; Savarese, M.; Pérez-Jiménez, Á. J.; Sancho-García, J. C.; Adamo, C. Range-separated double-hybrid functional from nonempirical constraints. *J. Chem. Theory Comput.* **2018**, *14*, 4052–4062.

(102) Leang, S. S.; Zahariev, F.; Gordon, M. S. Benchmarking the performance of time-dependent density functional methods. *J. Chem. Phys.* **2012**, *136*, 104101.

(103) Loos, P.-F.; Galland, N.; Jacquemin, D. Theoretical 0–0 energies with chemical accuracy. *J. Phys. Chem. Lett.* **2018**, *9*, 4646–4651.

(104) Grimme, S. In *Reviews in computational chemistry*; Lipkowitz, K. B., Boyd, D. B., Eds.; Wiley-VCH: New York, 2004; Vol. 20, pp. 153-218.

(105) Perdew, J. P. Density-functional approximation for the correlation energy of the inhomogeneous electron gas. *Phys. Rev. B* **1986**, *33*, 8822–8824.

(106) Vosko, S. H.; Wilk, L.; Nusair, M. Accurate spin-dependent electron liquid correlation energies for local spin density calculations: a critical analysis. *Can. J. Phys.* **1980**, *58*, 1200–1211.

(107) Koch, H.; Christiansen, O.; Jørgensen, P.; Sanchez de Merás, A. M.; Helgaker, T. The CC3 model: an iterative coupled cluster approach including connected triples. *J. Chem. Phys* **1997**, *106*, 1808–1818.

(108) Dunning, T. H. Gaussian basis sets for use in correlated molecular calculations. I. the atoms boron through neon and hydrogen. *J. Chem. Phys.* **1989**, *90*, 1007–1023.

(109) Kendall, R. A.; Dunning, T. H.; Harrison, R. J. Electron affinities of the first-row atoms revisited. systematic basis sets and wave functions. *J. Chem. Phys.* **1992**, *96*, 6796–6806.

(110) Brémond, É.; Pérez-Jiménez, Á. J.; Sancho-García, J. C.; Adamo, C. Range-separated hybrid density functionals made simple. *J. Chem. Phys.* **2019**, *150*, 201102.

(111) Alipour, M.; Karimi, N. Spin-opposite-scaled range-separated exchange double-hybrid models (SOS-RSX-DHs): marriage between DH and RSX/SOS-RSX is not always a happy match. *J. Chem. Theory Comput.* **2021**, published online, DOI: 10.1021/acs.jctc.1c00271 (accessed on 6 July 2021).

(112) Paci, I.; Johnson, J. C.; Chen, X.; Rana, G.; Popović, D.; David, D. E.; Nozik, A. J.; Ratner, M. A.; Michl, J. Singlet fission for dye-sensitized solar cells: can a suitable sensitizer be found? *J. Am. Chem. Soc.* **2006**, *128*, 16546–16553.

(113) Wen, J.; Havlas, Z.; Michl, J. Captodatively stabilized biradicaloids as chromophores for singlet fission. *J. Am. Chem. Soc.* **2015**, *137*, 165–172.

(114) Grotjahn, R.; Maier, T. M.; Michl, J.; Kaupp, M. Development of a TDDFT-based protocol with local hybrid functionals for the screening of potential singlet fission chromophores. *J. Chem. Theory Comput.* **2017**, *13*, 4984–4996.

(115) Masoomi-Godarzi, S.; Liu, M.; Tachibana, Y.; Goerigk, L.; Ghiggino, K. P.; Smith, T. A.; Jones, D. J. Solution-processable, solid state donor-acceptor materials for singlet fission. *Adv. Energy Mater.* **2018**, *8*, 1801720.

(116) Masoomi-Godarzi, S.; Liu, M.; Tachibana, Y.; Mitchell, V. D.; Goerigk, L.; Ghiggino, K. P.; Smith, T. A.; Jones, D. J. Liquid crystallinity as a self-assembly motif for high-efficiency, solution-processed, solid-state singlet fission materials. *Adv. Energy Mater.* **2019**, *9*, 1901069.

(117) Christiansen, O.; Koch, H.; Jørgensen, P. Perturbative triple excitation corrections to coupled cluster singles and doubles excitation energies. *J. Chem. Phys.* **1996**, *105*, 1451–1459.

(118) Loos, P.-F.; Scemama, A.; Blondel, A.; Garniron, Y.; Caffarel, M.; Jacquemin, D. A mountaineering strategy to excited states: highly accurate reference energies and benchmarks. *J. Chem. Theory Comput.* **2018**, *14*, 4360–4379.

(119) Loos, P.-F.; Scemama, A.; Boggio-Pasqua, M.; Jacquemin, D. Mountaineering strategy to excited states: highly accurate energies and benchmarks for exotic molecules and radicals. *J. Chem. Theory Comput.* **2020**, *16*, 3720–3736.

(120) Schäfer, A.; Horn, H.; Ahlrichs, R. Fully optimized contracted gaussian basis sets for atoms Li to Kr. *J. Chem. Phys.* **1992**, *97*, 2571–2577.

(121) Andersson, K.; Malmqvist, P. A.; Roos, B. O.; Sadlej, A. J.; Wolinski, K. Second-order perturbation theory with a CASSCF reference function. *J. Chem. Phys.* **1990**, *94*, 5483–5488.

(122) Angeli, C.; Pastore, M. The lowest singlet states of octatetraene revisited. *J. Chem. Phys.* **2011**, *134*, 184302.

(123) Platt, J. R. Classification of spectra of cata-condensed hydrocarbons. *J. Chem. Phys.* **1949**, *17*, 484–495.

(124) Lopata, K.; Reslan, R.; Kowalska, M.; Neuhauser, D.; Govind, N.; Kowalski, K. Excited-state studies of polyacenes: A comparative picture using EOMCCSD, CR-EOMCCSD(T), range-separated (LR/RT)-TDDFT, TD-PM3, and TD-ZINDO. *J. Chem. Theory Comput.* **2011**, *7*, 3686–3693.

(125) Grimme, S.; Parac, M. Substantial errors from time-dependent density functional theory for the calculation of excited states of large π systems. *ChemPhysChem* **2003**, *4*, 292–295.

(126) Parac, M.; Grimme, S. A TDDFT study of the lowest excitation energies of polycyclic aromatic hydrocarbons. *Chem. Phys.* **2003**, *292*, 11 – 21.

(127) Marian, C. M.; Gilka, N. Performance of the density functional Theory/Multireference configuration interaction method on electronic excitation of extended π-systems. *J. Chem. Theory Comput.* **2008**, *4*, 1501–1515.

(128) Richard, R. M.; Herbert, J. M. Time-dependent density-functional description of the 1La state in polycyclic aromatic hydrocarbons: charge-transfer character in disguise? *J. Chem. Theory Comput.* **2011**, *7*, 1296–1306.

(129) Kowalski, K.; Piecuch, P. New coupled-cluster methods with singles, doubles, and noniterative triples for high accuracy calculations of excited electronic states. *J. Chem. Phys.* **2004**, *120*, 1715–1738.

(130) Jacquemin, D.; Duchemin, I.; Blase, X. Is the Bethe-Salpeter formalism accurate for excitation energies? Comparisons with TD-DFT, CASPT2, and EOM-CCSD. *J. Phys. Chem. Lett.* **2017**, *8*, 1524–1529.

(131) Serrano-Andrés, L.; Fülscher, M. P. Theoretical study of the electronic spectroscopy of peptides. III. charge-transfer transitions in polypeptides. *J. Am. Chem. Soc.* **1998**, *120*, 10912–10920.

(132) Peach, M. J. G.; Benfield, P.; Helgaker, T.; Tozer, D. J. Excitation energies in density functional theory: an evaluation and a diagnostic test. *J. Chem. Phys* **2008**, *128*, 044118.

(133) Loos, P.-F.; Comin, M.; Blase, X.; Jacquemin, D. Reference energies for intramolecular charge-transfer excitations. *J. Chem. Theory Comput.* **2021**, *17*, 3666–3686.

(134) Weigend, F.; Ahlrichs, R. Balanced basis sets of split valence, triple zeta valence and quadruple zeta valence quality for h to rn: design and assessment of accuracy. *Phys. Chem. Chem. Phys.* **2005**, *7*, 3297–3305.

Graphical TOC Entry